Bull Volcanol (2014) 76:802
DOI 10.1007/s00445-014-0802-1

RESEARCH ARTICLE

Post 19 ka B.P. eruptive history of Ulleung Island, Korea, inferred from an intra-caldera pyroclastic sequence

G. B. Kim · S. J. Cronin · W. S. Yoon · Y. K. Sohn

Received: 28 August 2013 / Accepted: 23 January 2014 / Published online: 20 March 2014

Abstract Ulleung Island is a Quaternary volcanic island located in the mid-western part of the East Sea (Sea of Japan) back-arc basin, which has erupted from the Pliocene until the late Holocene. This study focuses on reconstructing the latest eruptive history of the island by describing the sedimentological and stratigraphic characteristics of the most recent, trachytic/phonolitic pyroclastic sequence, named the Nari Tephra Formation. This formation is preserved as a succession of unwelded pyroclastic and epiclastic deposits within an embayed margin of the Nari Caldera. The embayment acted as a topographic trap for proximal pyroclastic deposits, and contains a complete record of the past 19,000 years of eruption history. The formation includes evidence for five separate eruptive episodes (Member N-1 to N-5), with intervening weathered and/or soil horizons indicating hundreds to thousands of years of repose between each eruption. Eruption styles and depositional mechanisms varied between and during individual episodes, reflecting changing dynamics of the magma plumbing system, magmatic gas coupling, and a variable role of external water. Extra-caldera sequences show that only a few of these eruptions generated sustained eruption columns or pyroclastic density currents (PDCs) large enough to overtop the caldera wall. Thus tephra sequences outside the caldera provide an underestimate of eruption frequency, and care needs to be taken in the interpretation and correlation to distal tephra sequences recognized in marine and terrestrial records. In addition, topographic effects of caldera structures should be considered for the assessment of PDC-related hazards in such moderately sized pyroclastic eruptions.

Keywords Caldera · Eruptive episode · Tephra · Ulleung Island · Pyroclastic

Editorial responsibility: C. Oppenheimer

G. B. Kim
School of Earth and Environmental Sciences, Seoul National University, Seoul 151-742, South Korea

Y. K. Sohn (✉)
Department of Earth and Environmental Sciences and Research Institute of Natural Sciences, Gyeongsang National University, Jinju 660-701, South Korea
e-mail: yksohn@gnu.ac.kr

S. J. Cronin
Volcanic Risk Solutions, Massey University, Private Bag 11 222, Palmerston North, New Zealand

W. S. Yoon
Department of Earth and Marine Sciences/Marine and Environmental research Institute, Jeju National University, Jeju 690-756, South Korea

Introduction

Ulleung Island, located in the northern margin of the Ulleung Basin, the southwestern East Sea (Sea of Japan), is a Quaternary volcanic island whose activity stretches into the Holocene (<5.6 ka B.P.) (Kim 1985; Xu et al. 1998; Kim et al. 1999; Okuno et al. 2010) (Tables 1 and 2; Fig. 1). According to previous studies, the emergent portion of the volcano comprises basaltic/trachybasaltic to trachytic/phonolitic lavas, dikes, and volcaniclastic deposits which can be classified up to six eruptive stages on the basis of petrological and geochronological criteria (e.g., Yoon 1984; Yun 1986; Xu et al. 1998; Kim et al. 1999; Song et al. 1999) (Table 1). Although the details of the classification are still debated, it is commonly inferred that the latest one or two stages were the most explosive and produced large plinian eruptions with pumiceous tephras distributed throughout the East Sea and over the Japanese Islands (Arai et al. 1981; Machida et al. 1984).

For the last three decades, intensive tephrochronological studies on the latest explosive eruptions on Ulleung Island have been made on the basis of marine sediment cores and on-

Table 1 Stratigraphic classifications and petrochemical descriptions of Ulleung Island

Kim and Lee (1983) Min et al. (1988)	Kim (1985) Xu et al. (1998)	Won and Lee (1984)	Yun (1986)	Kim et al. (1999)	Yoon (1984)
Talus	Stage 5 Leucite-bearing trachyandesite lava and trachytic pyroclastics	Coastal terrace deposit	Post-caldera phase Tephra Leucite trachyandesite flows and cinder cone	Stage5 Leucite-bearing trachyandesite (0.1 Ma)	Alluvium
5th stage Leucite-bearing trachyandesite Caldera sediment		5th period Leucite trachyandesite			Caldera Deposit Albong Lava
Pumice, trachyandesitic pyroclastics, and welded tuff Marine terrace deposit	Stage 4 Trachytic pumice, ash, and lapilli (9,300–6,300 year BP*)	Pumice, trachyandesite tuff Intra-caldera deposit	Main phase Upper: Tephra related to caldera formation	Stage 4 Pyroclastics, tuff block, pumice, and ash	Ulleung Trachyte Group Trachytic and phonolitic lavas
4th stage Trachyte and phonolite	Stage 3 (0.58 Ma) Upper trachytic and phonolitic lavas Trachytic air fall deposits	4th period Kwanmobong Trachyte Daedung Trachyte	Middle: Trachyte and phonolite: extrusive domes, spines, and schlieren	Stage 3 Upper: Trachyte with basalt intrusion and trachyandesite (0.47–0.24 Ma)	
3rd stage Trachytic lava, agglomerate, tuff, and breccia	Middle trachytic and phonolitic lavas Trachytic air fall deposits Lower trachytic lavas	3rd period Trachyte agglomerate and lapilli tuff Cheonbudong Trachyte		Lower: Trachyte, trachyandesite, and phonolite (0.73–0.60 Ma)	
2nd stage Trachytic/trachyandesitic agglomerate, tuff, and dike	Stage 2 Trachytic agglomerate, lava, dike, and trachyandesitic lava (1.05 Ma)	2nd period Gadubong Phonolite Trachyte/trachyandesite agglomerate and lapilli tuff	Lower: Trachyte: flows and pyroclastics	Stage 2 Trachyte, trachybasalt, and trachyte agglomerate (0.83–0.77 Ma)	Sataegam Fm. Conglomerates and sandstones
1st stage Basaltic agglomerate, tuff, lava, and dike (2.7–1.8 Ma)	Stage 1 Trachybasaltic agglomerate, lava, and dike (1.37–1.40 Ma)	1st period Basalt lava, agglomerate, and lapilli tuff	Pre-erosion phase Basaltic flows, dikes, and pyroclastics	Stage 1 Basaltic agglomerate and lava, picritic basalt, and trachyte (1.37–0.97 Ma)	Dodong Basalt Fm. Basaltic pillow lavas and hyaloclastites
				Jeodong Formation Tuffaceous sandstones and conglomerates	Sadong Breccia Fm. Trachytic/trachyandesitic breccias and lavas
					Basement

Age data of ^{14}C dating after Machida et al. (1984) and Arai et al. (1981)

Table 2 Comparison of the Ulleung tephrostratigraphy in variable localities

Ulleung Island			East Sea (Sea of Japan)			Japanese Islands		
Machida et al. (1984)	Okuno et al. (2010) Shiihara et al. (2011)	Im et al. (2012)	Arai et al. (1981)	Chun et al. (1997, 1998)	Domitsu et al. (2002)	Kitagawa et al. (1995)	Nagahashi et al. (2004)	Higashino et al. (2005)
U-1								
K-Ah* (6.3 ka B.P.)		Nari-III (<5.6 cal ka B.P.)						
U-2	U-2 (5.6 cal ka B.P.)			Ulleung-I (<5.9 ka B.P.)				
	K-Ah[a]						BT-3	Hm-6
U-3	U-3 (8.3–9 cal ka B.P.)	Nari-II (8.4 cal ka B.P.)			TRG1 (8.4 cal ka B.P.)		BT-4	Hm-2 (7.7–8 ka B.P.)
U-4	U-4 (11.0 cal ka B.P.)		U-Oki (9.3 ka B.P.)	Ulleung-II (9.3 ka B.P.)	TRG2 (10.0 cal ka B.P.)	Unnamed (10.7 cal ka B.P.)	BT-5	
		Nari-I (18.8 cal ka B.P.)						
AT (21.0–22.0 ka B.P.)								
U-5				Ulleung-III				
U-6								
U-7								

Values in parentheses are ^{14}C ages of Ulleung Island tephras obtained from variable terrestrial and marine sites in Ulleung Island, Japanese Islands, and the East Sea

[a] The stratigraphic position of the K-Ah ash, suggested by Machida et al. (1984), was later modified by Shiihara et al. (2011)

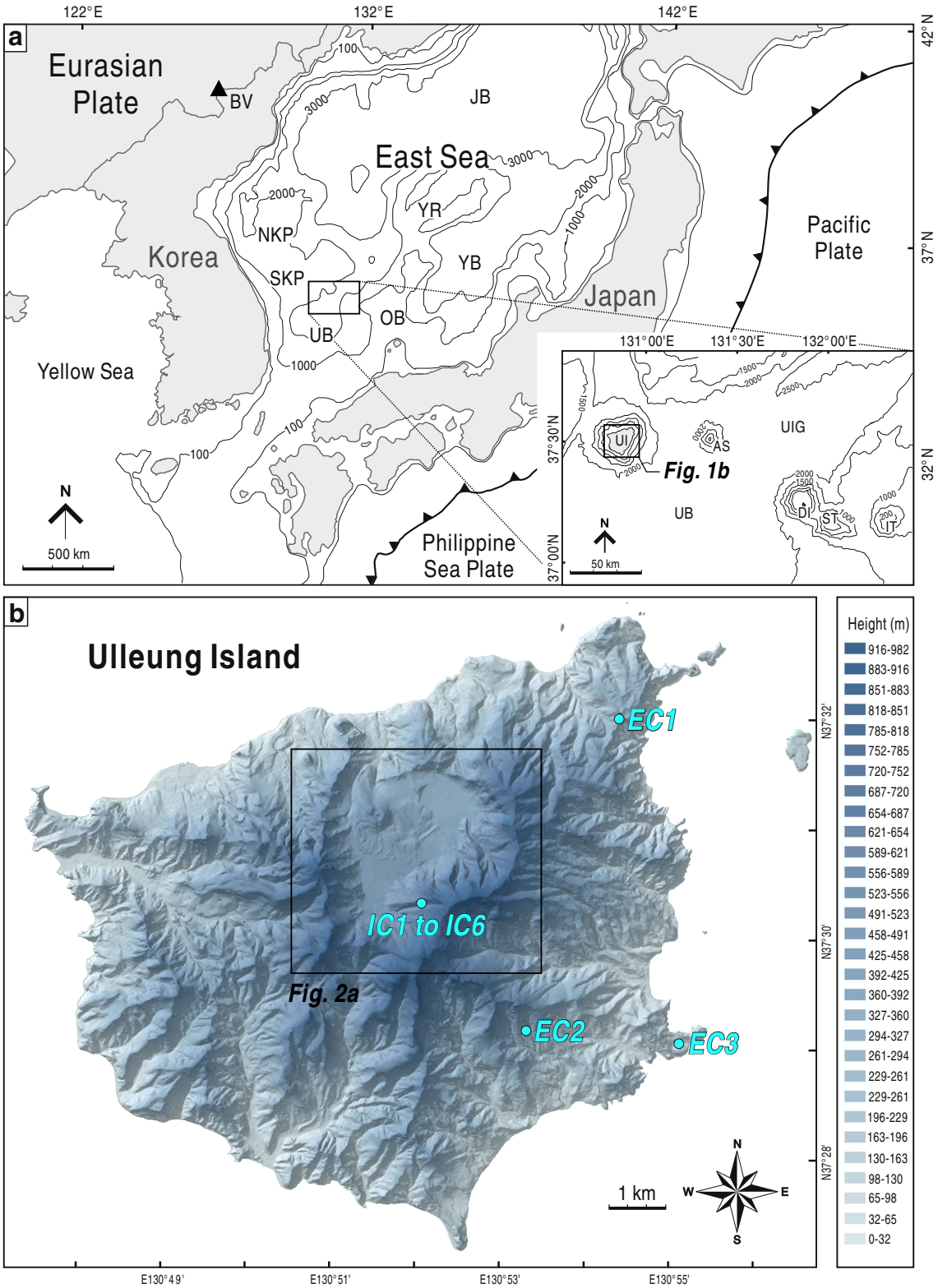

Fig. 1 **a** Physiographic map of the East Sea (Sea of Japan) showing the location of Ulleung Island. *UI* Ulleung Island, *AS* Anyongbok Seamount, *ST* and *IT* Shimheungtaek and Isabu tablemounts, *BV* Baekdusan Volcano, *JB*, *UB* and *YB* Japan, Ulleung, and Yamato basins, respectively, *OB* Oki Bank, *SKP* and *NKP* South and North Korea Plateau, respectively, *YR* Yamato Rise. **b** DEM of Ulleung Island showing topography and the study locations

land investigation around the East Sea. These studies established the stratigraphic framework of the Ulleung tephras together with the other tephras from various eruptive sources around the eastern Eurasian margin (e.g., U-Oki ash from Ulleung Island, Aira-Tn ash from the Aira Caldera, Kikai-Akahoya ash from the Kikai Caldera, Baekdusan-Tm ash from the Baekdusan Volcano) (c.f., Arai et al. 1981; Machida et al. 1984; Miura et al. 1991; Domitsu et al. 2002). Owing to the distinctive trachytic/phonolitic chemical composition, which is rare in the arc-related tephra records of the Japanese Islands, the tephras from Ulleung Island are readily distinguished from the other tephras sourced from volcanoes in the Japanese Islands (e.g., AT and K-Ah ashes), as well as from the Baekdusan Volcano in the north of the Korean Peninsula (e.g., Baekdusan-Tm ash) (Machida et al. 1984; Chun et al. 1997; Park et al. 2007) (Fig. 1). The individual tephra layers sourced from Ulleung Island show uniform major oxide compositions of volcanic glass shards, enabling detailed correlation of the marine tephras with proximal terrestrial members, especially with the assistance of radiocarbon ages (Shiihara et al. 2011). These extensive works on the tephras provide an ever-improving tephrochronology as well as a guide to understanding the recent volcanic history of Ulleung Island.

Despite ongoing efforts to correlate these tephra layers, the details of volcanic eruption styles and transport/depositional mechanisms of the tephras on Ulleung Island are virtually undescribed because marine and terrestrial tephras hitherto studied are fragmentary, and correlation of medial–distal thin fallout layers to proximal deposits has not been systematically made. For these reasons, we report on a detailed study of the proximal deposits of the most recent explosive eruptions of Ulleung Island. We use this to examine aspects of the pyroclastic eruptions and their depositional mechanisms, leading to new insights into future potential volcanic hazards from Ulleung Island. We define the Nari Tephra Formation as a succession of tephra that includes the latest phonolitic and trachytic eruption products, deposited inside the caldera of Ulleung Island. We present here a new comprehensive stratigraphic framework for pyroclastic deposits inside and immediately outside the caldera, as well as an evaluation of the eruption styles and depositional processes for each eruptive episode identified. This sequence also provides new information on the range of topographic influences on pyroclastic density current (PDC) sedimentation, particularly intracaldera deposition and re-deposition processes.

Geological setting

Ulleung Island is located within a Cenozoic volcanic field along the northern margin of the Ulleung Basin (37°30′N, 130°52′E) in the southwestern part of the East Sea (Fig. 1). Previous geological/geophysical studies suggest that multiaxial back-arc extension caused deep subsidence of the sea bed since the Early Oligocene (c. 32 Ma) in association with vigorous multistage volcanic activities (Lallemand and Jolivet 1985; Jolivet 1986; Kimura and Tamaki 1986; Tamaki and Honza 1991; Tamaki et al. 1992). Volcanism during the back-arc evolution of the Ulleung Basin can be classified into three stages based on volcano–stratigraphic relationships (Kim et al. 2011). The stage 1 volcanism included fissure-type eruptions triggered by initial back-arc rifting during the Early Miocene (c. 20 Ma). This was followed by stage 2 eruptions sited along an ENE–WSW trending chain of volcanic edifices during the Middle Miocene (17–11 Ma). Stage 3 volcanism is characterized by multiple eruptions probably from the Late Miocene through to the Holocene (11 Ma–5.6 ka B.P.), building volcanic seamounts and islands, i.e., Ulleung and Dok islands, the Anyongbok Seamount, and the Shimheungtaek and Isabu tablemounts (Fig. 1a). Previous dating studies using K-Ar and radiocarbon methods on these volcanoes and stratigraphic reconstructions made from seismic reflection studies on the Ulleung Basin suggest that among these volcanoes Ulleung Island is the youngest and has been active until at least the mid-Holocene (c.f., Sohn and Park 1994; Okuno et al. 2010; Kim et al. 2011; Im et al. 2012; Kim et al. 2013). Several hypotheses have been proposed to explain the tectono-volcanic origin of the island, including a mantle plume, dehydration melting associated with subduction of the Pacific Plate, and decompressional melting by back-arc extension (Peng et al. 1986; Min et al. 1988; Basu et al. 1991; Tatsumoto and Nakamura 1991; Kim et al. 2011).

The entire Ulleung volcanic edifice rises about 3,000 m from the seafloor, of which the emergent portion is 982 m in height and 72.6 km^2 in area. The island exposes a range of basaltic lavas and related epiclastic deposits, through to trachytic domes and flows. The most recent volcanism was concentrated within the caldera of the volcano, named Nari Caldera. This 2.8-km-diameter caldera has an amphitheater-like shape open to the north and shows embayed topography in the south (Fig. 1). The semicircular rim bordering the caldera rises <100 m above the caldera floor in the north and reaches up to 600 m in the south (Fig. 2). The northwestern part of the caldera is occupied by a lava dome/tephra cone complex, Albong, which rises about 140 m from the caldera floor (Fig. 2).

The island consists of basaltic/trachybasaltic to trachytic/phonolitic lavas and volcaniclastic deposits, which have been subdivided into three to six stages with different stratigraphic classifications and petrochemical descriptions in previous works (Table 1). K-Ar dated stages included the following: 2.7±0.9 to 1.37±0.04 Ma basaltic lavas and basaltic agglomerates, 1.05±0.02 Ma trachytic agglomerate, 0.83±0.01 to 0.60±0.01 Ma lower trachyte, 0.58±0.01 to 0.24±0.01 Ma upper trachyte, and <0.01 Ma trachyandesite (Min et al. 1988; Xu et al. 1998; Kim et al. 1999; Song et al. 2006). Radiocarbon

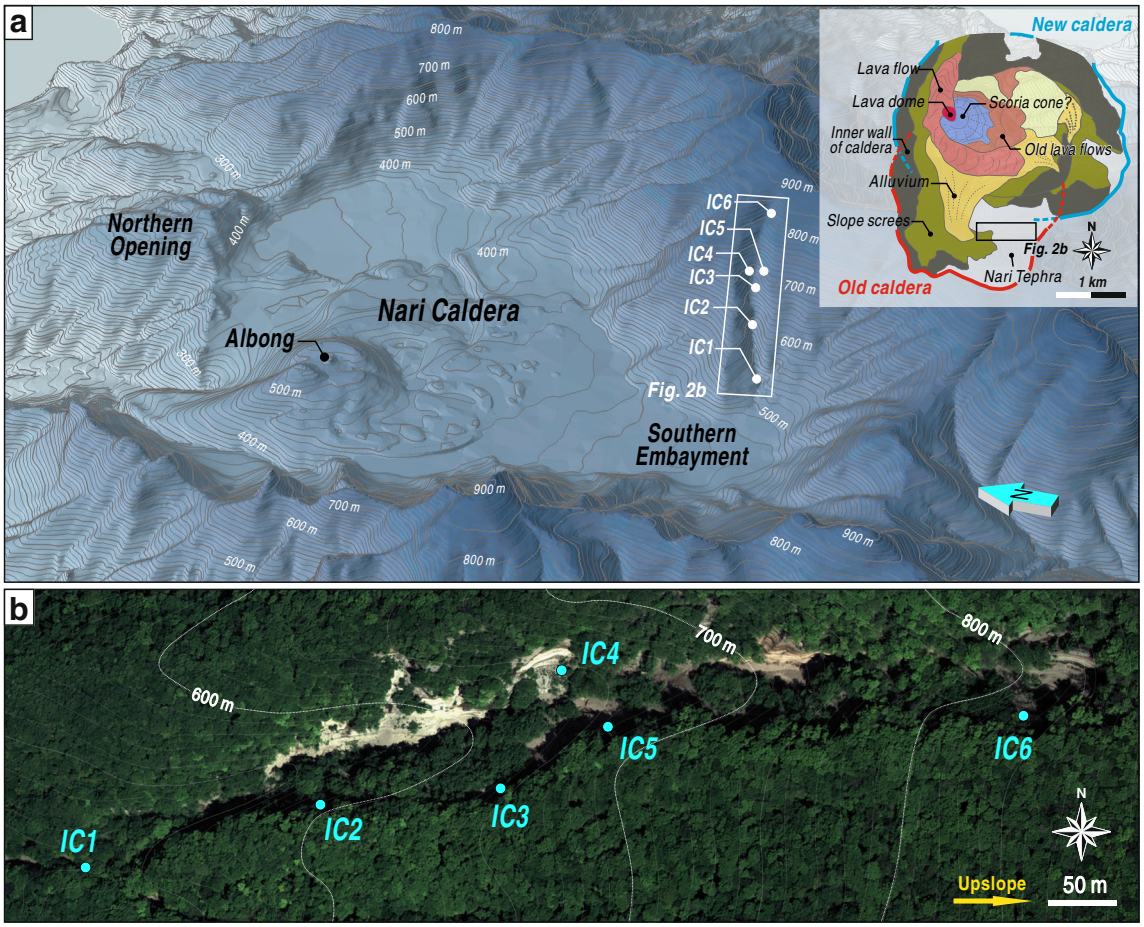

Fig. 2 **a** DEM showing the topography of the Nari Caldera and study locations. *Inset* illustrates the distribution of sediment/rock types inside the caldera (modified after Machida et al. 1984). **b** Aerial photograph of study area showing the sites of outcrop measurement

ages of the latest volcanic activity were first reported to date between c. 9.3 to 6.3 ka B.P. on the basis of marine sediment cores from the East Sea (Arai et al. 1981; Machida et al. 1984). Recently, Okuno et al. (2010) reported radiocarbon dates of c. 11, 9, and 5.6 ka B.P. for a series of extra-caldera tephra layers using charcoal and pumiceous soil samples. Meanwhile, Im et al. (2012) reported ^{14}C dates of ~19, 8.5, and 8.4–7 ka B.P. for a series of intra-caldera pyroclastic deposits.

Review of Ulleung tephrostratigraphy

Several workers have attempted to establish correlations between the terrestrial and marine tephra layers that are found on Ulleung Island, below the East Sea, and throughout the Japanese Islands on the basis of radiocarbon ages and chemical compositions (Arai et al. 1981; Machida et al. 1984; Kitagawa et al. 1995; Chun et al. 1997; Domitsu et al. 2002; Nagahashi et al. 2004; Higashino et al. 2005; Okuno et al. 2010; Shiihara et al. 2011; Im et al. 2012) (Tables 2 and 3). Machida et al. (1984) defined seven tephra layers (U-1 to U-7 in descending order) from the extra-caldera sites on Ulleung Island and constrained their ages based on two time-marker tephra layers, i.e., the Aira-Tn ash (21–22 ka B.P.) and the Kikai-Akahoya ash (6.3 ka B.P.). Later, Okuno et al. (2010) and Shihara et al. (2011) revised the tephrostratigraphy based on radiocarbon ages and geochemical analyses of volcanic ash, thereby defining the ages of the U-4 as ~11 ka B.P., U-3 as 8.3 to 9 ka B.P., and U-2 as 5.6 ka B.P.

The U-4, U-3, and U-2 tephras, found at many extra-caldera sites in the eastern to southern part of the island, mainly comprise trachytic or phonolitic pumice and contain amphibole, clinopyroxene, and alkali feldspar as common phenocrysts (Shiihara et al. 2011). All these tephras have the characteristics of fall deposits, of which the details are described by Okuno et al. (2010). The U-4 tephra is 0.8 to 1.0 m thick in total, comprising a normally graded, grayish white pumice along with lithic fragments in the lower part (unit U-4a) and a gray layer of lithic and scoria lapilli in the upper part (unit U-4b). The U-3 tephra is 0.7 to 1.1 m thick in total, comprising grayish brown to white ash and fine pumice deposit at the base (unit U-3a), grayish white accretionary lapilli-bearing tuff in the middle (unit U-3b), and a bed of normally graded, grayish white pumice and lithic lapilli at the top (unit U-3c). The U-2 tephra is 0.3 to 1.1 m thick in total, comprising grayish yellow

Table 3 Results of AMS ^{14}C dating

Sampling site		Stratigraphic position	Material	$\delta^{13}C$ (‰)	^{14}C date (BP)	Lab nr [sample ID]	Age range (cal BP) [2σ, probability %]
Intra-caldera site (Im et al. 2012 and this study)	N37°37′18″ E130°51′55″	In N-5	Charcoal	–22.91	16,460±110	SNU12-R108	19,493–19,933 [95.4]
				–23.5	15,560±100	[C1]	18,690–18,990 [95]
				–22.6	15,880±60	[C2]	18,960–19,150 [95]
	N37°29′50″ E130°51′58″	In N-3	Charcoal	–24.1	7,600±40	[C3]	8,360–8,440 [95]
	N37°29′50″ E130°51′58″	In N-3	Charcoal	–23.7	7,660±40	[C4]	8,390–8,540 [95]
Extra-caldera site (Okuno et al. 2010)	N37°32′17″ E130°54′6″	In U-2	Charcoal	–25.4	4,910±35	5494	5,590–5,666 [85.39]
				–25.5	4,965±35	5495	5,604–5,749 [97.01]
				–23.9	4,945±35	5496	5,602–5,738 [100]
				–23.8	4,940±35	5497	5,600–5,734 [100]
	N37°31′6″ E130°54′10″	Beneath U-2	Soil	–27.0	4,710±30	7730	5,323–5,417 [52.11]
	N37°31′54″ E130°56′13″	Beneath U-3	Soil	–28.1	7,525±35	6755	8,301–8,405 [92.14]
	N37°31′6″ E130°54′10″	Beneath U-3	Soil	–25.1	8,030±35	6756	8,846–9017 [70.93]
	N37°31′54″ E130°56′13″	Beneath U-4	Soil	–27.5	9,786±35	6752	11,177–11,126 [100]
	N37°31′6″ E130°54′10″	Beneath U-4	Soil	–24.5	12,165±40	6754	13,890–14,141 [100]
				–27.5	11,840±45	7309	13,581–13,816 [100]
	N37°31′54″ E130°56′13″	Beneath U-4	Charcoal	–27.0	12,030±40	6764	13,781–13,996 [100]
				–26.5	12,090±40	6765	13,819–14,051 [100]
				–26.5	12,095±40	6766	13,822–14,056 [100]

to white accretionary lapilli-bearing tuff in the lower part (unit U-2a) and normally graded, gray to white beds of pumice and lithic lapilli in the upper part, which are overlain by black soil.

Shiihara et al. (2011) proposed an integrated stratigraphic framework for Ulleung tephras on the basis of eruption ages and petrographic characteristics. The U-4 tephra was correlated to the U-Oki tephra from several sites in the East Sea and on land in Japan. This marker tephra has been reported in many studies with different codes (e.g., Ulleung-II, TRG2 and Hane Pumice and BT-5) (Chun et al. 1997; Domitsu et al. 2002; Nagahashi et al. 2004). Tephras correlated with the U-3 and U-2 deposits are occasionally reported as indistinct layers of scattered pumice and/or volcanic glass-rich ash outside the island. The TRG1, BT-4, and Hm-2 tephras are regarded as correlatives of the U-3 tephra, and the Ulleung-1 tephra as a correlative of the U-2 tephra (Chun et al. 1997; Chun et al. 1998; Domitsu et al. 2002; Nagahashi et al. 2004; Higashino et al. 2005).

Materials and methods

Detailed field observations and sedimentary logs of the Nari Tephra Formation were collected both inside and outside the caldera (Figs. 1 and 2). The sedimentary logs were measured at a scale of 1:20 to include bed thickness, grain size, texture, sedimentary structure, and componentry. For petrological and geochemical analysis, pumice samples were collected from each eruptive member of the Nari Tephra Formation exposed in both intra- and extra-caldera sites (Figs. 1 and 2). For radiocarbon dating, charcoal samples were collected from the lowermost eruptive member of the intra-caldera tephra formation. The charcoal samples were analyzed using the Accelerator Mass Spectrometer (AMS) technique in the National Center for Inter-University Research Facilities, Seoul National University.

Characteristics of the intra-caldera Nari Tephra Formation

A succession of the Nari Tephra Formation, about 70 m thick, is exposed along a valley incised roughly parallel to the southern inner wall of the Nari Caldera (Fig. 2). The formation can be divided into five members, N-5 to N-1 in ascending order. Each unit is bounded by either a prominent erosion surface or soil horizon indicative of a significant hiatus between eruptions (Fig. 3). The members comprise pumiceous

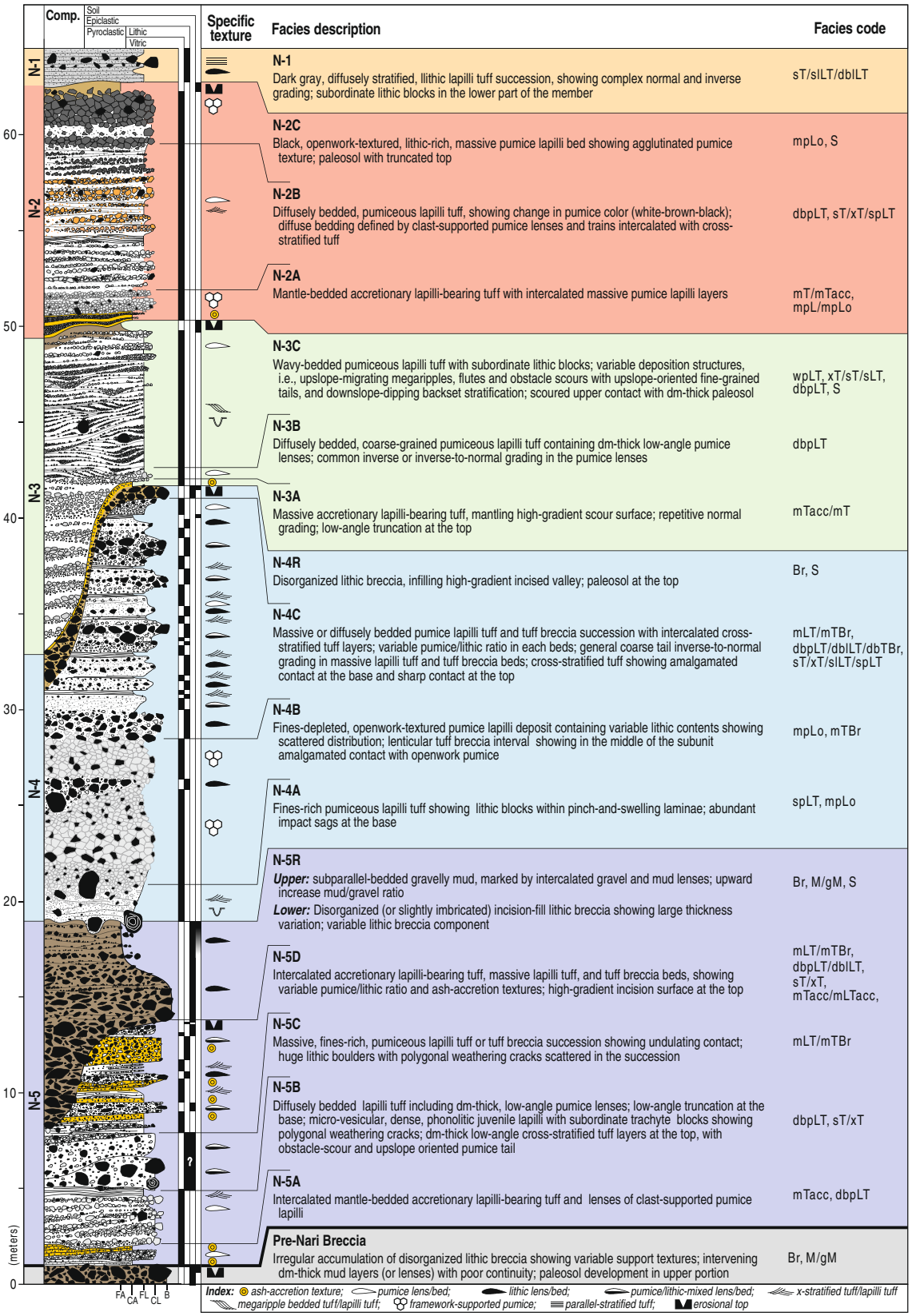

Fig. 3 Sedimentary log of the Nari Tephra Formation from intra-caldera sites IC1 to IC6

lapilli tuff mostly of phonolitic composition with subordinate lithic clasts of variable origins. A total of 19 lithofacies are defined and summarized in Table 4. Grain size terminology used here follows White and Houghton (2000).

Pre-Nari Breccia

Description

The Nari Tephra Formation is underlain by an irregular stack of lithic breccia beds (Br), characterized by variable bed geometries, clast support fabrics, and clast orientations (Fig. 4). Individual breccia beds commonly have a discontinuous wedge geometry (2 to 4 m in max. thickness) and are intercalated with decimeter-thick gravel-bearing mud lenses. Breccias are generally composed of coarse lapilli to block-sized trachyte clasts which are overall angular, but slightly rounded along their edges. The matrix comprises poorly sorted gravel-bearing sandy mud with reddish to brownish coloration due to diagenesis. The top of the breccia succession is marked by irregular truncation (Fig. 4).

Interpretation

In the geological map of the Nari Caldera (inset of Fig. 2a), along-strike distribution of thick breccia successions on the slope face of the inner caldera wall and ubiquitous alluvium near the base of slope suggest that the Nari Caldera was subjected to continual slope failure in association with sporadic centripetal drainage process. The irregular stack of breccia wedges of the Pre-Nari Breccia is, likewise, attributed to repetitive accumulation of debris upon screes fringing the inner caldera wall during a long repose period of volcanic eruption. Gravel-rich mud layers, draping the breccia wedges, are interpreted as deposits of water-laid epiclastic mud and gravel transported by temporary overland flows on the screes mostly in response to heavy rainfall and/or snowmelt events.

Member N-5

Description

The lowermost member of the Nari Tephra Formation is marked by a variety of lithofacies, and divided into five units: N-5A to N-5D and N-5R in ascending order (Fig. 3). The member comprises medium lapilli to block-sized trachytic pumice with accidental trachyte blocks. Juvenile pumice clasts are characterized by very low vesicularity and abundant acicular feldspar microphenocrysts in the groundmass (Fig. 5).

Unit N-5A is 1 to 1.5 m thick and composed of massive accretionary lapilli-bearing tuff (mTacc) with intercalated lenses or mounds of diffusely bedded pumiceous lapilli tuff (dbpLT). The accretionary lapilli-bearing tuff beds are 5–50 cm thick, and mantle the irregular top of the underlying Pre-Nari Breccia and diffusely bedded pumiceous lapilli tuff beds (Fig. 4b).

Unit N-5B consists of diffusely bedded pumiceous lapilli tuff (dbpLT) which includes decimeter-thick lenses of clast-supported lapilli and blocks (Fig. 4c). The unit has a low-angle truncating relationship with the underlying unit and shows wide thickness variation due to subsequent erosion. Juvenile lapilli and blocks are phonolitic in composition (Brenna et al. 2014), commonly angular in shape, light gray to dark gray in color, and marked by bimodal vesicularity distribution between micro-vesicular (commonly <1 mm in vesicle diameter lacking bubble wall texture) and non-vesicular (Fig. 5). The unit contains subordinate trachyte blocks as an accidental lithic component. The lapilli tuff is transitionally overlain by 5- to 30-cm-thick, low-angle cross-stratified tuff (sT/xT) (Fig. 4c).

Unit N-5C is a c. 3-m-thick, fines-rich massive pumiceous lapilli tuff (mLT) or tuff with a low-angle truncation surface at the base (Fig. 4d). Large portion of pumice clasts are severely altered to show an orange/deep brown color. Accidental large trachyte and tuff blocks, often exceeding 50 cm in diameter, are scattered within the deposit and show accompanying asymmetric bedding sags near the base (Fig. 4a, d). In the middle to upper part of the unit, diffusely stratified lapilli tuff locally infills troughs with upslope-dipping stratification (Fig. 4d).

Unit N-5D is a c. 6-m-thick succession, comprising mantle-bedded accretionary lapilli-bearing tuff (mTacc), massive pumiceous lapilli tuff showing variable ash-accretion textures (mLTacc), and massive lithic and pumiceous lapilli tuff or tuff breccia with subtle horizontal clast orientation (mLT/mTBr) (Fig. 4d). A variety of ash-accretion textures occur in different beds, including accretionary lapilli and ash pellets (Fig. 4e), armored lapilli (Fig. 4f), and vesiculated lapilli tuff (Fig. 4g). The unit is truncated by a high-gradient and high-relief incision surface incising through the entire stack of underlying units (Fig. 4h).

Unit N-5R is a chaotic succession of lithic breccias (Br) overlying the incision surface (Fig. 4h). The breccias are commonly poorly sorted, and either clast- or matrix-supported with indistinct imbrication. The upper portion of the unit is marked by intercalation of 10- to 30-cm-thick, commonly lenticular, mud and gravelly mud layers (M/gM) (Fig. 4i).

Interpretation

The accretionary lapilli-bearing tuff, intercalated with pumice lapilli beds in unit N-5A, suggests that the eruption initiated with fluctuating phreatomagmatic explosions that generated steam-rich eruption clouds and unsteady pulses of PDCs. The poorly vesicular and micro-vesicular juvenile lapilli and blocks, comprising the major component of unit N-5B,

Table 4 Major lithofacies of the Nari Tephra Formation

Facies code	Description	Occurrence	Interpretation
mLT/mTBr	Massive lapilli tuff or tuff breccia showing variable grading pattern, clast support texture, sorting, and pumice/lithic ratio	N-4C, N-4B, N-5D, N-5C	Deposition from dense and non-turbulent PDCs or en mass deposition of concentrated granular underflow at the basal level of density-stratified PDCs; apparent inverse or inverse-to-normal grading by dispersive pressure
dbpLT/dblLT/ dbTBr	Diffusely bedded, lithic or pumiceous lapilli tuff or tuff breccia including low-angle lenses or trains of clast-supported pumice or lithic clasts	N-1, N-2B, N-3C, N-3B, N-4C, N-5D, N-5B, N-5A	Deposition from density-stratified and pulsating PDCs segregating granular underflow or floatsam of pumice or lithic lapilli from the current; waxing or waning of currents indicated by occasional coarsening- or fining-up pattern within a lapilli tuff or tuff breccia interval
sT/ xT/spLT/slLT	Decimeter-thick layers of stratified or cross-stratified, pumiceous or lithic tuff or lapilli tuff, showing transitional contact with underlying massive or diffusely bedded lapilli tuff or tuff breccia and wavy-bedded pumiceous lapilli tuff beds	N-1, N-2B, N-3C, N-4C, N-4A, N-5D, N-5B	Tractional deposition from low-concentrated, fully dilute, turbulent pyroclastic surges following the highly concentrated PDC deposition; commonly occurring in the final phase of single PDC pulse
mT/mTacc/ mLTacc	Massive tuff or fine lapilli tuff often showing variable ash-accretion textures, i.e., massive accretionary lapilli-bearing tuff (Fig. 4e), massive armored lapilli-bearing lapilli tuff (Fig. 4f), and massive vesiculated lapilli tuff (Fig. 4g)	N-2A, N-3A, N-5D, N-5A	Ashfall or co-ignimbrite fall deposits from steam-rich eruption cloud or PDCs from phreatomagmatic eruptions; fluctuation in water content in the eruption cloud indicated by alternation of mT and mTacc facies; occasional deposition of armored lapilli-bearing or vesiculated lapilli tuff (mLTacc) from PDCs containing abnormally large water content
mpL/mpLo	Massive, fines-poor (or fines-depleted) pumiceous lapilli deposit marked by good sorting and angular shape of pumice clasts with occasional agglutinated and openwork texture; mantling topography with occasional impact sags near the base	N-2C, N-2A, N-4B, N-4A	Air fall pumice from plinian or subplinian eruption cloud with accompanied ballistic lithic projectiles
wpLT	Wavy-bedded and fines-rich pumiceous lapilli tuff marked by upslope-migrating megaripples and flutes or obstacle scours with upslope-oriented cluster of fine pumiceous lapilli	N-3C,	Deposition from energetic, turbulent PDCs in which deposition is dominated by traction and saltation; dominant upslope-oriented current direction indicated by megaripple bedform, cluster bedform, and flutes or obstacle scours
Br	Clast-supported and disorganized (or slightly imbricated) lithic breccia commonly showing trough-fill or incision-fill bed geometry	N-4R, N-5R, Pre-Nari Breccia	Slope scree near the foot of the caldera wall or debris-flow or debris-fall deposits infilling incised valley during inter-eruptive stage
M/gM	Mud or gravelly mud layer commonly draping lithic breccia	N-5R, Pre-Nari Breccia	Water-laid mud or gravelly mud from sporadic drainage system along the valleys on the caldera slope
S	Paleosol with low-angle erosional top	N-2C, N-3C, N-4R, N-5R	Weathered interval Indicative of non-deposition for a substantial period of time

T tuff, *LT* lapillit tuff, *Br* breccia, *M* mud, *S* soil, *m* massive, *db* diffusely bedded, *ds* diffusely stratified, *s* stratified, *x* cross-stratified, *p* pumiceous, *l* lithic, *g* gravel-rich, *w* wavy-bedded, *o* openwork-textured, *acc* accretionary lapilli-bearing

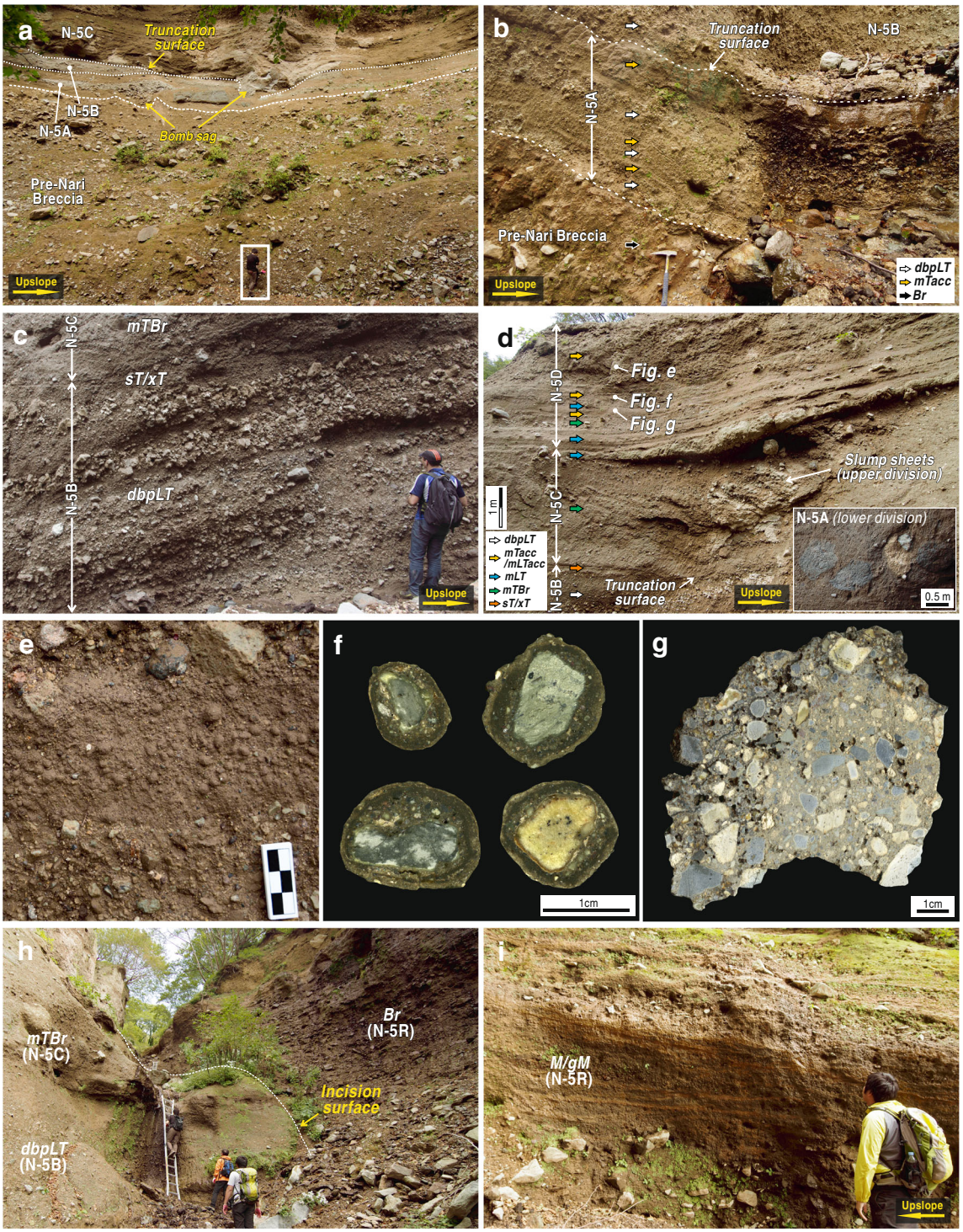

Fig. 4 Outcrop photographs showing the deposit features of Member N-5 at site IC2. **a** Overview of Pre-Nari Breccia. *Person in white rectangle* gives the scale. **b** Basal part of Member N-5 marked by alternating massive pumiceous lapilli tuff and accretionary lapilli-bearing tuff layers mantling the weathered/eroded top of Pre-Nari Breccia. Hammer (c. 30 cm long) gives the scale. **c** Clast-supported pumice lenses in diffusely bedded pumiceous lapilli tuff of unit N-5B. **d** Complex alternations of massive lapilli tuff or tuff breccia and accretionary lapilli tuff beds in units N-5C and N-5D. **e**–**g** Close-up of variable ash-accretion textures in unit N-5D, respectively, showing the details of an accretionary lapilli-bearing tuff layer and the cross sections of armored lapilli and vesiculated tuff. **h** Lithic breccia succession in the lower part of unit N-5R showing diffuse imbrication of lithic blocks. **i** Stratified mud and gravelly mud interval in the upper part of unit N-5R

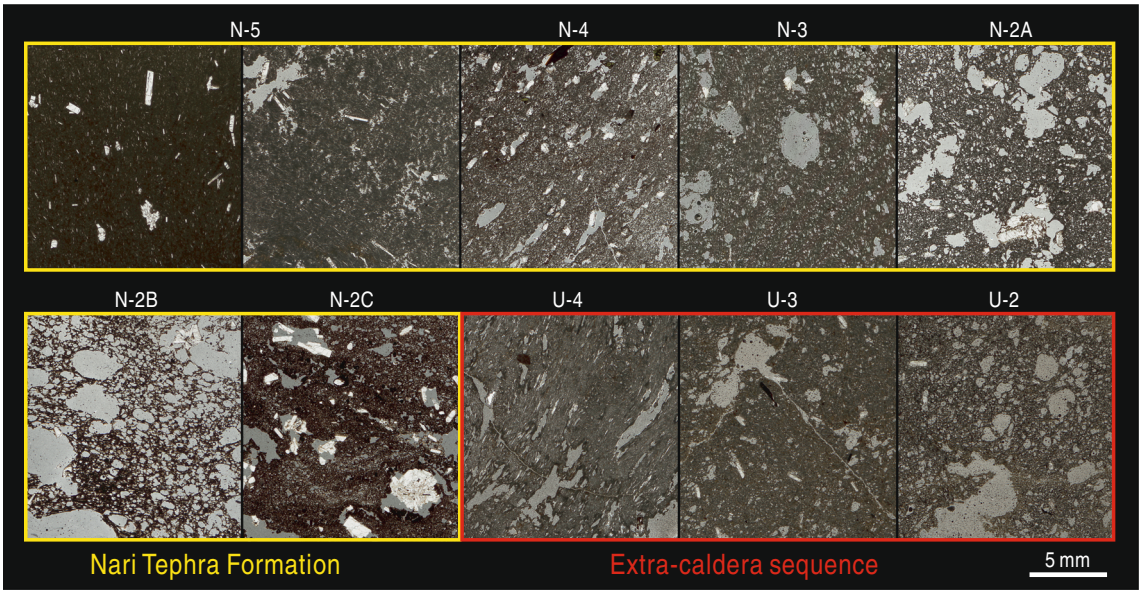

Fig. 5 Scanned thin-section images of juvenile lithic and pumice clasts from intra- and extra-caldera tephra sequences. Note that the pumices from Member N-4, N3, and N-2A have identical vesicle textures to those of U-4, U-3, and U-2 tephras

suggest extremely low magmatic gas expansion and inefficient magmatic fragmentation during the eruption, which may not fall under the realm of either magmatic or phreatomagmatic fragmentation process. The micro-vesicular and microlite-rich juvenile clasts suggest that the source magma of Member N-5 was probably emplaced as an endogeneous dome or cryptodome or a shallow conduit fill, which experienced over-pressurization in response to microlite crystallization prior to the explosive eruptions (Sparks 1997; Hammer et al. 1999). The accidental trachyte blocks are interpreted to have derived from the earlier trachytes comprising the summit of the volcano. This trachyte, which probably had been capping the endogeneous dome or cryptodome, was probably disintegrated and transported over the inner caldera wall either ballistically or by high-concentration PDCs during phreatomagmatic eruptions or sudden explosive disintegration of the over-pressurized dome (Sparks 1997). It is inferred that the bimodal vesicularity distribution of juvenile clasts is due to non-uniform volatile loss from an initially homogeneous magma (c.f., Hoblitt and Harmon 1993). The clast-supported lapilli lenses in this unit suggests segregation of dense basal layers of coarse lapilli and blocks from a PDC that fluctuated in current intensity or competence (Branney and Kokelaar 2002).

The massive lapilli tuff containing large lithic blocks (N-5C) is interpreted as deposits of dense and laminar PDCs accompanied by ballistically transported lithic blocks that were probably derived from the conduit or vent wall. The trough-filling lapilli tuff with diffuse upslope-dipping stratification (Fig. 4d) is attributed to syn-depositional remobilization or down-slope slippage of unconsolidated deposits on steep slope. Several massive tuff beds in unit N-5D showing a range of ash-accretion textures suggest variable physical properties and water contents of the PDCs that originated from sporadic phreatomagmatic activities (c.f., Schumacher and Schmincke 1991; Rosi 1992; Houghton et al. 2000) (Fig. 4e–g). The massive lapilli tuff or tuff breccia beds in this unit may have partly resulted from syn-eruptive reworking processes. The amalgamated transitional contacts between tuff, lapilli tuff, and tuff breccia beds suggest continuous aggradation of these beds without significant depositional hiatus.

The high-gradient erosional surface incising into the underlying units (N-5D to N-5A) suggests a prolonged eruptive hiatus after the cessation of the eruption. The breccia beds of unit N-5R are interpreted as the deposits of debris flows or debris falls that originated from caldera-wall collapse and remobilization of loose volcaniclastic materials. The mud-rich upper part of the unit is interpreted to have formed by draping of water-laid mud and gravel in the later stage of incision fill.

Member N-4

Description

Member N-4 is a c. 23-m-thick succession of pumice lapilli, lapilli tuff, tuff, and tuff breccia that can be divided into four units: N-4A to N-4C and N-4R in ascending order (Table 4; Figs. 3, 6). Pumice clasts in this member have tubular vesicles with thin vesicle walls (Fig. 5).

The lowermost unit N-4A is a succession of c. 1-m-thick, pumiceous lapilli tuff, marked by gradual facies change from lithic-rich pumiceous lapilli tuff showing diffuse pinch-and-

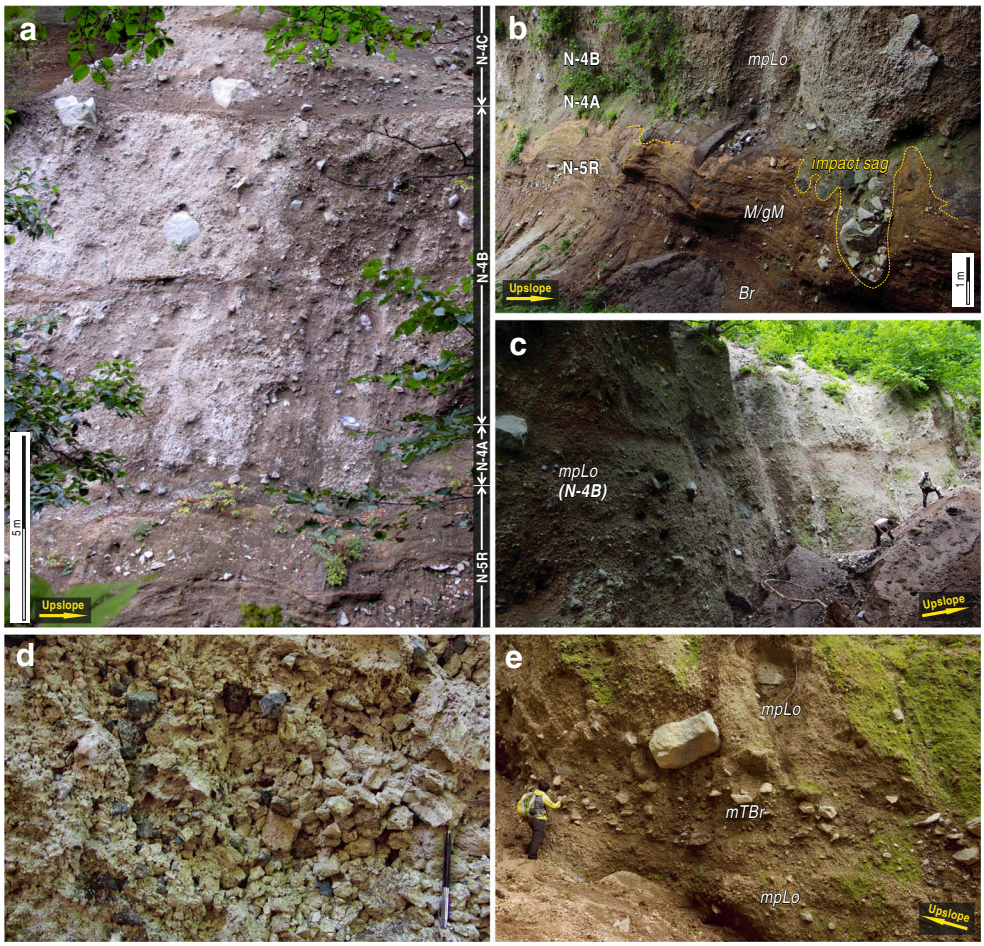

Fig. 6 Outcrop photographs showing the deposit features of Member N-4 at site IC3. **a** Overall view of Member N-4 and the uppermost part of Member N-5, showing the stratigraphic relationships between depositional units. **b** Basal contact between Member N-5 and N-4 showing huge lithic blocks in an impact sag. **c** View of very crudely bedded unit N-4B. **d** Photograph showing the openwork texture of pumice and lithic clasts in unit N-4B. **e** Massive tuff breccia bed in the middle part of unit N-4B

swelling stratification near the base (spLT) to massive, openwork pumice lapilli deposit (mpLo) in the upper part. Huge lithic blocks, often exceeding 1 m in diameter, produced deep impact sags below them (Fig. 6b).

Unit N-4B is a c. 8-m-thick, crudely bedded, openwork pumice lapilli deposit (mpLo) (Fig. 6c), which is overall fines-poor and consists mainly of medium lapilli-sized pumice clasts and scattered lithics of variable lithologies (e.g., trachytes, syenites, sedimentary rocks, metamorphic rocks, and etc.) (Fig. 6d). Discontinuous and poorly sorted tuff breccia (mTBr) occurs in the middle part of the unit, showing diffuse lower and upper contacts (Fig. 6e).

Unit N-4C is a ~13-m-thick, lithic block-rich and matrix-supported pumiceous lapilli tuff succession, having a sharp but non-erosional contact with the underlying N-4B (Fig. 6a). It comprises a stack of 1 to 2 m-thick, massive or diffusely bedded, lithic-rich lapilli tuff and/or tuff breccia beds (mLT/dbpLT/dblLT/dbTBr/mTBr), interlayered with 10 to 20 cm thick stratified or cross-stratified tuff or lapilli tuff layers (sT/xT/spLT/slLT) (Figs. 3, 7). The lapilli tuff and tuff breccia facies generally coexist within a single bed due to lateral variations in clast contents, sorting, and ratios of pumice/lithic clasts (Fig. 7b). The diffuse stratification of lapilli tuff and tuff breccia beds is generally defined by trains or lenses of lithic or pumice clasts (Fig. 7a, b). In several massive tuff breccia beds, coarse lithic blocks are concentrated in the middle or upper part of the beds, showing inverse or inverse-to-normal grading (Fig. 7a, b). The cross-stratified tuff commonly overlies underlying lapilli tuff beds with transitional contacts (Fig. 7b, c). The beds of this unit as a whole are characterized by onlapping stratal geometry upon the inclined depositional surface with the overall beds thinning and terminating upslope (Fig. 7a). Relatively fine-grained parts of beds show stoss-erosional to stoss-depositional dune-like structures and climbing megaripples that apparently migrate upslope (Fig. 7b, c). This unit is capped by a 10- to 20-cm-thick paleosol at the top (Fig. 7a) and is overlain by lithic breccias (N-4R) with a high-relief incision surface in between.

Interpretation

Unit N-4A, with a fine ash-rich matrix and low-angle, swelling laminae, can be interpreted as the deposit from a pyroclastic surge occurring during the opening stage of the Member N-4 eruption. Abundant large lithic blocks and a gradual facies change into fines-poor openwork pumice lapilli deposit

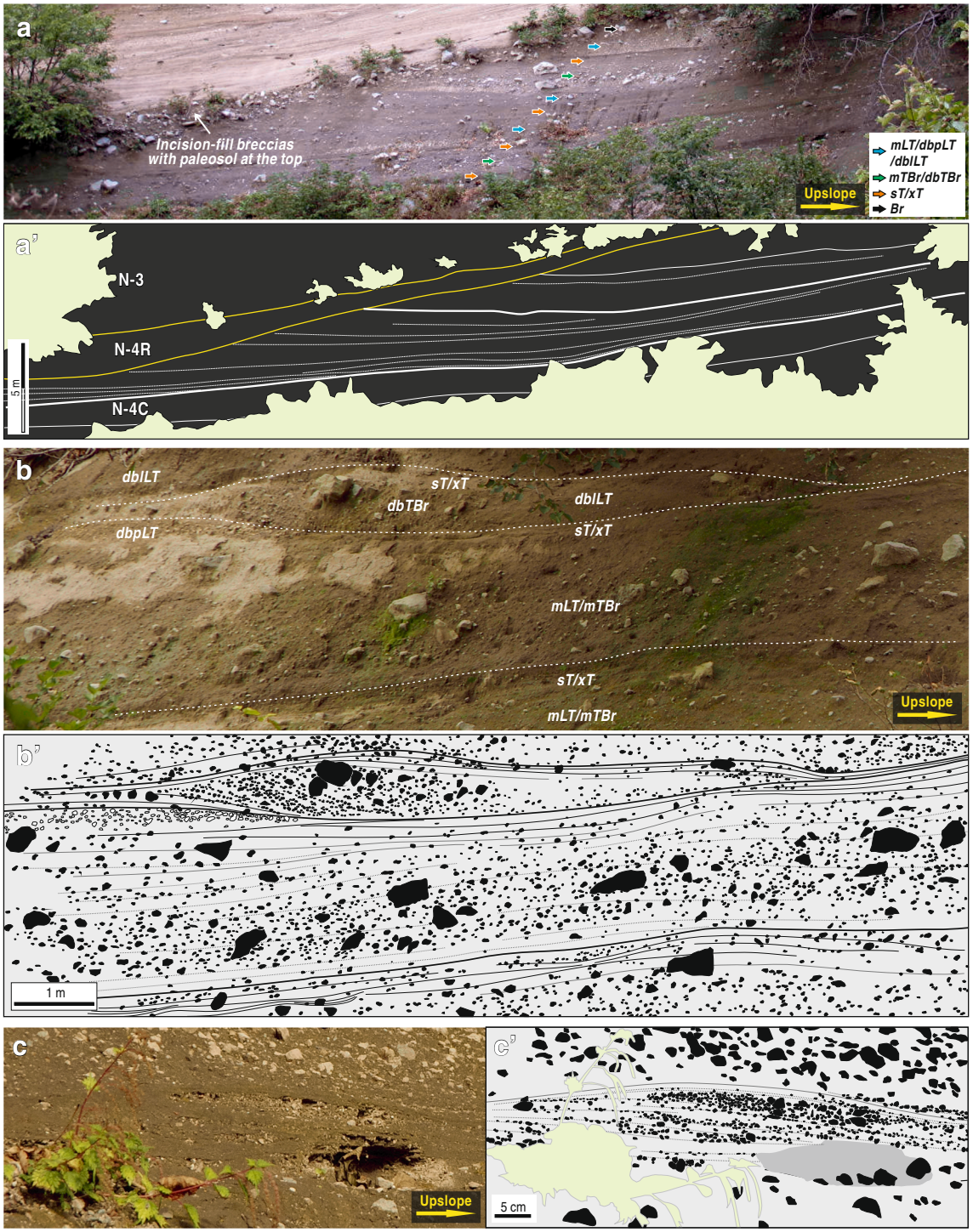

Fig. 7 **a** Photograph and line drawing of unit N-4C at site IC4, showing onlapping stratal geometry upon the inclined depositional surface with the overall beds thinning and terminating upslope. **b** Photograph and outcrop sketch of unit N-4C showing stoss-erosional to stoss-depositional dune-like structures. Inverse-to-normal grading is prominent in the bed at center. **c** Photograph and sketch of stratified tuff in unit N-4C showing climbing megaripples migrating upslope

suggests rapid widening of the vent and wet-to-dry transition of eruption style (Houghton et al. 2000). Unit N-4B lacks any features related to traction sedimentation, thus suggesting rapid aggradation of pumice fallout from a plinian eruption cloud, from which fine ash was efficiently winnowed by wind. The abundance of lithic clasts of variable lithologies suggests that wall rocks were commonly plucked from various levels of the conduit, which were subsequently transported as ballistic

projectiles (Wilson and Walker 1985; Allen 2001). The intervening massive tuff breccia in the unit is interpreted to have been transported by a highly concentrated, energetic PDC, representing partial collapse of plinian eruption column or a conduit-widening eruptive event. Subtle clast size variation in this unit is attributed to temporal variation of eruption intensity.

The lapilli tuff and tuff breccia beds of unit N-4C are interpreted as deposits of highly concentrated and block-rich PDCs followed by dilute and finer grained tails of the currents. The diffuse stratification, defined by lithic/pumice lenses or trains, suggests fluctuation of flow competence in a single PDC, in which coarse lithic or pumice clasts were segregated and concentrated. The subtle inverse or inverse-to-normal grading identified in several massive tuff breccia beds might have been caused by dispersive pressure in the high-concentration basal portion of PDCs. Lateral variation of grading pattern, stratification, and lithic clast contents in a single massive bed is attributed to non-uniformity of the current. The cross-stratified tuff showing diffuse contact with the underlying lapilli tuff/tuff breccia beds are interpreted as tractional deposits from more dilute PDCs that mark the waning phases of the PDC pulses. An abundance of coarse lapilli- to block-sized lithic clasts are interpreted as vent- or conduit-derived lithic ejecta entrained in energetic PDCs. The overall upslope-onlapping stratal termination together with upslope-migrating dunes or megaripples suggests gradual filling of the slope by the PDCs advancing toward the caldera wall. The capping paleosol layer and high-gradient incision surface at the top of the unit indicate a significant repose period with valley re-incision following the eruption.

Member N-3

Description

Member N-3 is a succession of 8- to 16-m-thick pumiceous lapilli tuff that can be divided into three units: N-3A to N-3C, based on their facies associations (Table 4; Figs. 3, 8). The pumice clasts in this member are characterized by elliptical, slightly stretched vesicles with thin vesicle walls (Fig. 5).

The lowermost unit N-3A is a 30- to 40-cm-thick accretionary lapilli-bearing tuff bed (mTacc), mantling the high-gradient incision surface above Member N-4. It was severely eroded before deposition of unit N-3B (Fig. 8b). The unit is well-sorted and shows multiple repeated pattern of normal grading which defines crude stratification.

Unit N-3B is a diffusely bedded pumiceous lapilli tuff containing decimeter-thick clast-supported pumice lenses (dbpLT) (Fig. 8a, c). This unit has a valley-filling geometry with onlap stratal termination against the high-gradient incision surface above Member N-4. Individual pumice lenses are composed of well-sorted, subangular pumice lapilli and blocks with subordinate accidental trachyte and syenite clasts, showing inverse or inverse-to-normal grading (Fig. 8c). Some stacks of pumice lenses have dune-like geometry with a retrograding stacking pattern (Fig. 8d).

Unit N-3C is a wavy- or megaripple-bedded pumiceous lapilli tuff (wpLT), of which the maximum thickness is c. 8 m (Figs. 2, 8a). This unit is mainly composed of coarse ash- to lapilli-grade, subrounded to rounded pumice clasts with subordinate lithic clasts, some of which form impact sags (Fig. 8e). Diverse structures are found in the unit including upslope-migrating megaripple bedforms, backset stratification that dips upslope relative to the bedding plane, and flute and obstacle scour marks with upslope-oriented fine-grained pumice tails (Fig. 8a, e).

Interpretation

Deep incision and soil development on the top of Member N-4 suggests a significant repose period before the eruption of Member N-3. Mantle-bedded accretionary lapilli-bearing tuff at the unit's base is interpreted to be a tephra fall deposit from initial vapor-rich phreatomagmatic activity. This was followed by a brief pause in eruption, inferred from the eroded top of the unit.

We interpret the diffusely bedded lapilli tuff of unit N-3B as a deposit from density-stratified PDCs, from which granular underflows were selectively deposited under fluctuating current competence. Upslope-stacking of pumice lenses suggests deposition from uphill-traveling PDCs, in which concentrated basal portions comprising large pumice/lithic clasts both moved upslope and avalanched locally downslope (Jeon et al. 2011).

The wavy-bedded lapilli tuff of unit N-3C by contrast was probably deposited from turbulent pyroclastic surges, which exerted strong shear stress on the bed to result in both depositional and erosional structures. Irregular bed thickness and grain size variation are attributed to the unsteadiness and non-uniformity of the pyroclastic surges. The migration directions of dunes, megaripples, flutes, and obstacle scours (Fig. 8a, d, e) suggest that the current moved overall upslope.

Member N-2

Description

Member N-2 is a succession of ~15-m-thick, diffusely bedded and/or massive pumiceous lapilli tuff units characterized by distinct changes of pumice colors from white, brown, to black (Figs. 3, 9). The member can be divided into four units, i.e., N-2A to N-2D, depending on the lithofacies association (Fig. 3). Pumice clasts show inflated bubble wall-type vesicle textures (N-2A and 2B) and micro-vesicular textures, as well as including abundant feldspar glomerocrysts (N-2C) (Fig. 5).

The lowermost unit N-2A is a ~2-m-thick succession marked by alternation between massive accretionary lapilli-

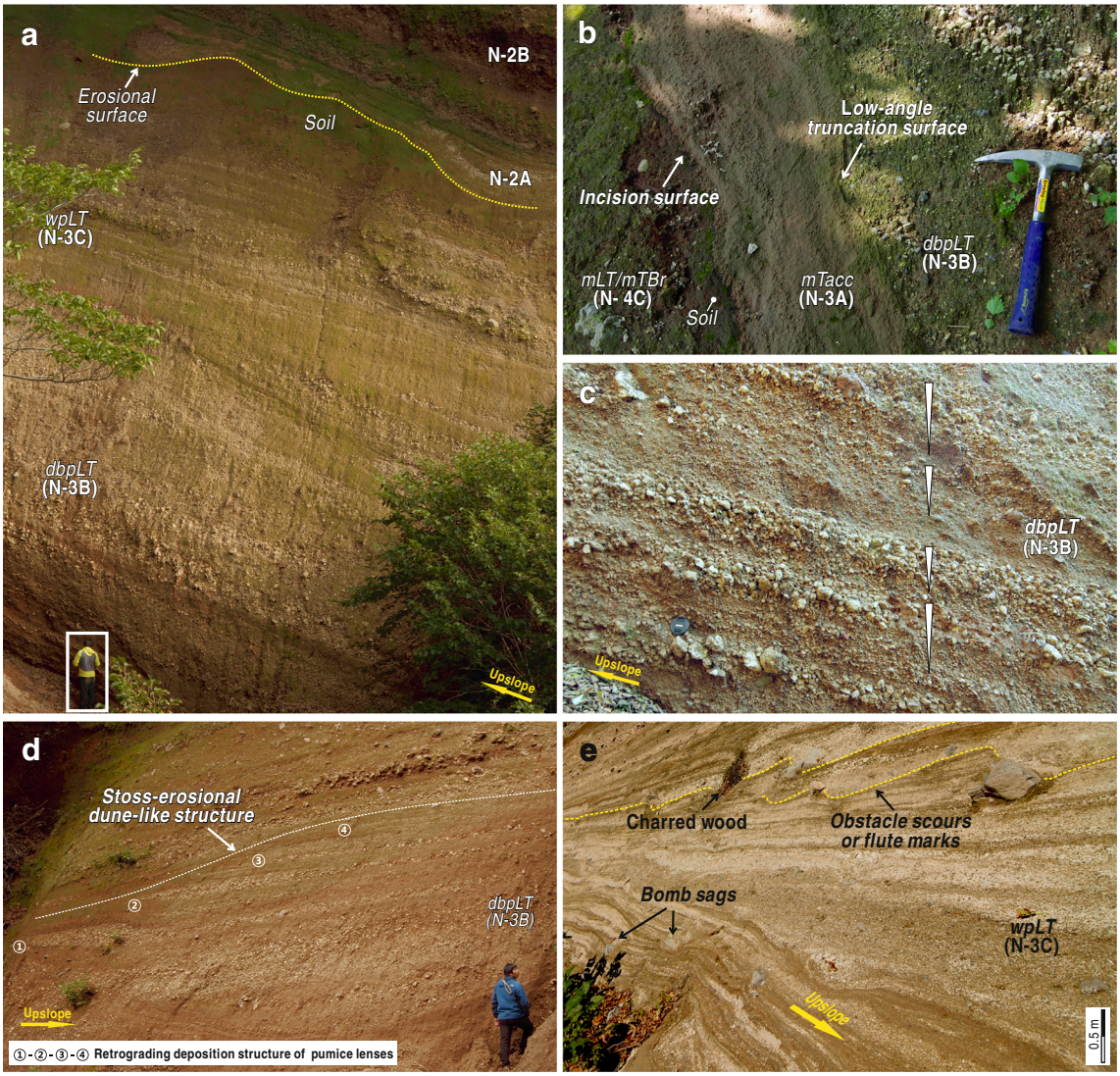

Fig. 8 Outcrop photographs showing the deposit features of Member N-3. **a** Overall view of Member N-3 and the lowermost part of unit N-2 at site IC5. Person in rectangle gives the scale. **b** Basal accretionary lapilli-bearing tuff of unit N-3A at site IC4. **c** Low-angle pumice lenses showing inverse grading in unit N-3B at site IC5. **d** Diffusely bedded pumiceous lapilli tuff showing dune-like stacking pattern of pumice lenses prograding upslope at site IC6. **e** Wavy-bedded pumiceous lapilli tuff of unit N-3C showing variable upslope-oriented flutes and obstacle scours at site IC4

bearing tuff (mT/mTacc) and fines-poor pumice lapilli (mpL) layers including subordinate accidental lithic lapilli (trachytes and phonolites) (Figs. 2, 9b). The intercalating layers show upwards increases in the abundance and clast size of pumice lapilli, which pass into massive deposits of openwork pumice lapilli (mpLo) (Fig. 9b). These alternating layers show mantling bed geometry and extensive lateral continuity with uniform bed thickness (Fig. 9b).

Unit N-2B is composed of decimeter-thick diffusely bedded pumiceous lapilli tuff (dbpLT), including clast-supported pumice lenses or trains with intervening uniform-thick (5 to 10 cm) tuff layers. The unit is characterized by distinctive color changes of pumice, from white, brown, to black in the lower, middle, and upper parts, respectively (Fig. 9a). In spite of the abrupt color change, the contacts between units are diffuse and transitional (Fig. 9a).

Unit N-2C consists of a ~3-m-thick massive, fines-depleted and black pumiceous lapilli deposit, containing common lithic clasts (more than seen in underlying units) (Fig. 9a). The unit shows an openwork deposit texture with pumice and obsidian clasts being partly agglutinated or welded (Fig. 9c). The topmost part of the unit is characterized by pale brown pumice lapilli, bounded by undulated erosional surface (Fig. 9d).

Interpretation

Alternation of accretionary lapilli-bearing tuff and fine-grained pumiceous tuff beds at the base of the member (unit

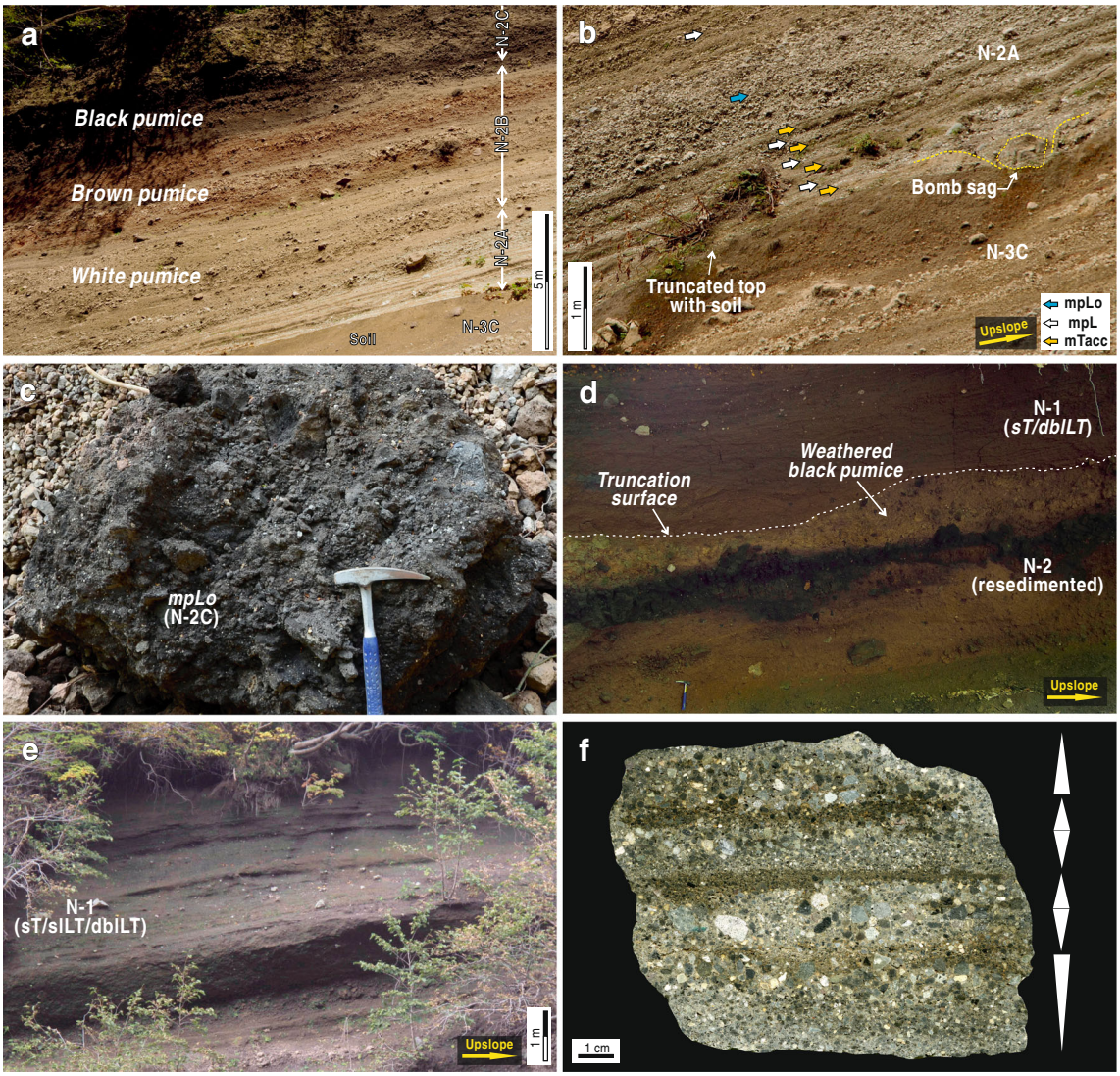

Fig. 9 Outcrop photographs showing the deposit features of Member N-2 and N-1. **a** Overall view of Member N-2 at site IC4. **b** Alternating accretionary lapilli-bearing tuff and openwork pumice in unit N-2A. **c** Agglutinated black pumice/obsidian and lithic lapilli in unit N-2C. **d** Erosional contact between Member N-2 and N-1 at site IC1, at which subparallel strata of Member N-1 show onlap stratal termination against the irregular truncation surface outlining the top of the altered black pumice of Member N-2. **e** Overall view of Member N-1 at the site IC4. **f** Polished slab photograph of diffuse parallel-stratified lapilli tuff in Member N-1, showing variable grading patterns

N-2A) suggests that the initial eruption fluctuated between phreatomagmatic and magmatic styles. The uniform thickness and mantling geometry of the tuff beds suggests fallout from a plinian eruption cloud. The diffusely bedded pumiceous lapilli tuff in unit N-2B, marked by interlayering clast-supported pumice lenses and stratified tuff, is interpreted to record more or less sustained but unsteady PDCs, in which basal granular underflow was segregated from dilute upper surges.

The different-colored pumices of this member have been shown to have identical chemical composition (Im et al. 2011), which implies that they do not represent different magmatic zones. The conspicuous pumice color change from white to black may instead reflect variations in oxidation of iron in the erupting pumice, and/or variations in the thickness of vesicle walls, and glass microlite content (Paulick and Franz 1997; Wilson and Houghton 2000). The agglutinated black pumice and obsidian clasts of unit N-2C suggest fallout of partially molten and degassed lapilli probably from a lava fountaining phase of eruption in the later stages of the episode (Wilson and Houghton 2000). The pale brown pumice color of the uppermost part of the member suggests pedogenic alteration of black pumice with accompanying erosional processes during a long depositional hiatus.

Member N-1

The uppermost member of the Nari Tephra Formation is up to 7 m thick at the study location (Figs 3, 9e). This member

consists of coarse ash- to medium lapilli-grade black vesicular juvenile clasts and lithic clasts of variable lithologies. The unit shows thin, continuous, diffuse, subparallel stratification (sT/sLT) defined by superposition of variably graded thin layers (Fig. 9f). This stratified tuff onlaps against the irregular eroded top of the black pumice deposits of Member N-2 (Fig. 9d). The juvenile clasts of Member N-1 are marked by abundant plagioclase and hornblende phenocrysts in a devitrified vesicular groundmass.

Interpretation

The high fine ash content of this unit along with crude but thin and continuous stratification defined by alternating normal and inverse-graded layers suggest traction-carpet deposition from more or less dilute, pulsating PDCs (Sohn 1997). Onlap stratal termination upon the black pumice deposit of Member N-2 with an erosional contact shows that there was a considerable time gap between the eruptions of the two members, during which loose volcaniclastic materials of unit N-2 were resedimented and pedogenically altered.

Characteristics of extra-caldera tephra layers

A 12-m-thick tephra succession was artificially exposed at the site EC1 (37°32′07″N, 130°54′24″E; Fig. 1b), which is located c. 2.4 km northeast from the present caldera rim. The lower 9 m of the succession is highly weathered, hampering sedimentological observations and geochemical analysis, whereas the upper 4 m comprises fairly fresh juvenile pumice. The uppermost 2.5 m could be divided into three tephra intervals by intervening soil layers and correlated with the U-4, U-3, and U-2 tephras of the previous tephrostratigraphic framework and with Member N-4, N-3, and N-2 of the Nari Tephra Formation, respectively (Fig. 10).

U-4 tephra (Unit N-4B)

Description

U-4 tephra is a c. 0.8-m-thick (locally several meters thick at other sites) succession of openwork pumice lapilli overlain by weathered pumiceous lapilli tuff (Figs. 10 and 11). The unweathered lower part of the tephra comprises coarse lapilli- to block-size pumice and lithic clasts with accompanying impact sags near the base (Fig. 11d). The weathered upper part consists of massive tuff including diffuse lenses of pumice lapilli with an eroded top. Pumice clasts in this tephra are commonly angular in shape, and characterized by contorted and tubular vesicle textures (Fig. 5). Lithic clasts have variable lithologies probably of different origins, i.e., vent wall-derived trachytes and subvolcanic syenites or monzonites (Fig. 11f).

Interpretation

The fines-depleted, openwork texture and the abundance of deep conduit-derived lithic clasts (syenite and monzonite clasts) suggest fallout of pumice from a plinian column, along with impact of ballistic lithic ejecta. This distinctive deposit character and clast lithology of U-4 tephra is identical to that of unit N-4B of the Nari Tephra Formation, implying that these tephra units inside and outside the caldera originated from same eruption event. The absence of the stratigraphic equivalent of unit N-4C at this site suggests that the block-rich PDCs, which followed the initial plinian pumice-fall, could not transport tephra beyond the caldera rim.

Radiocarbon dating and stratigraphic relationships with several marker tephras, which originated from Japanese Islands (e.g., AT and K-Ah ashes), suggest that the U-4 tephra (unit N-4B of the Nari Tephra Formation) is a stratigraphic equivalent of the U-Oki tephra in the East Sea and Japanese Islands (Machida et al. 1984; Shiihara et al. 2011) (Table 2).

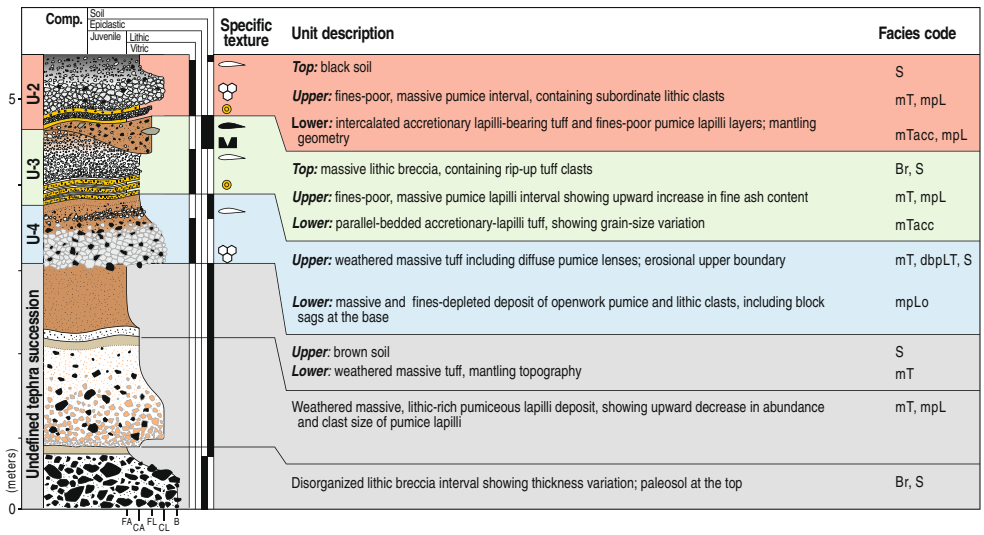

Fig. 10 Sedimentary log of the extra-caldera tephra sequence from site EC1

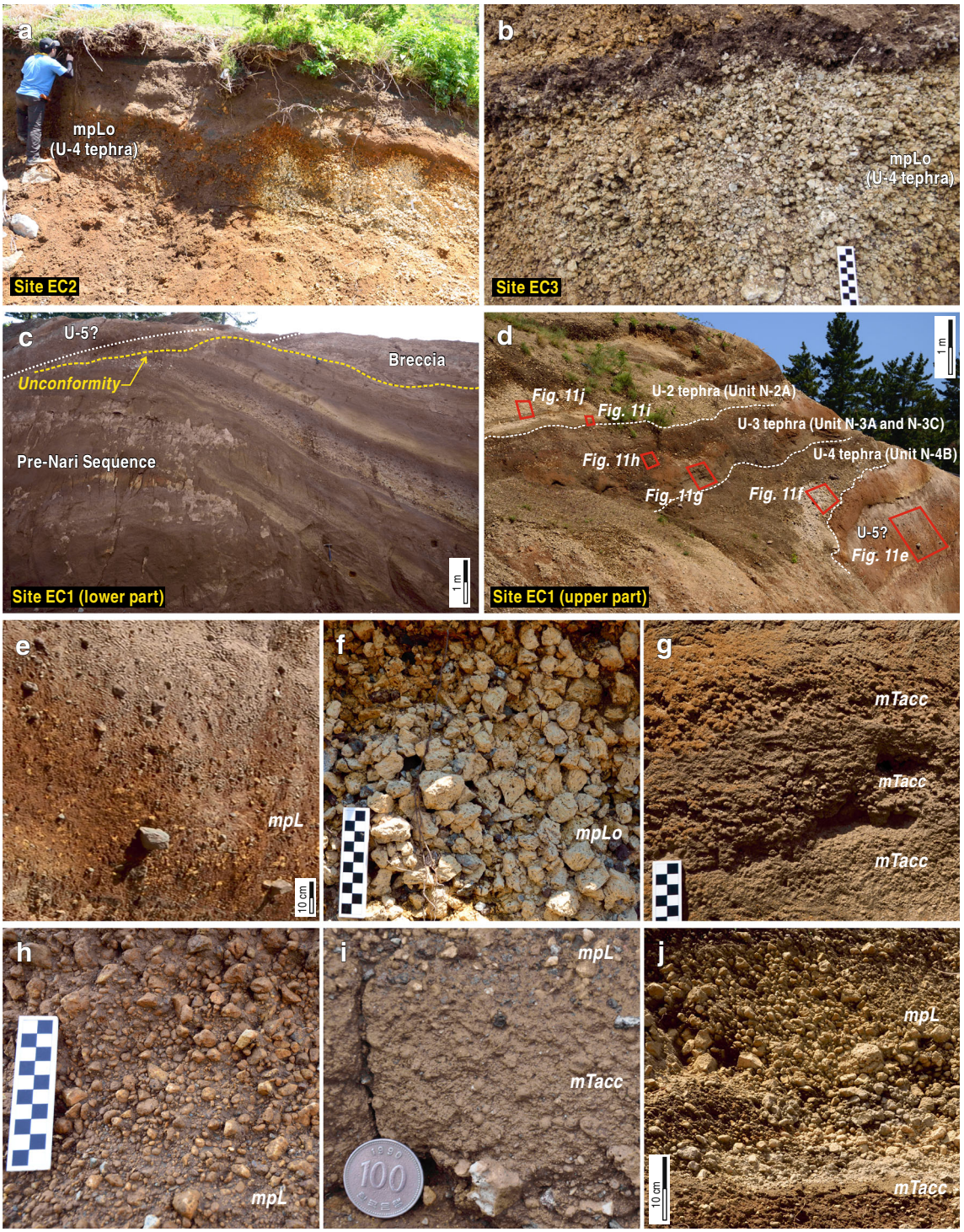

Fig. 11 Outcrop photographs showing the deposit features of the extra-caldera tephra sequence. **a** Outcrop exposure at site EC2. **b** Outcrop exposure at site EC3. **c** The old tephra sequence, predating the Nari Tephra Formation at site EC1. **d** Overall view of extra-caldera tephra sequence, stratigraphic equivalent of the intra-caldera Nari Tephra Formation at site EC1. **e** Lithic-rich pumiceous lapilli tuff, probably a stratigraphic equivalent of intra-caldera Member N-5. **f** Massive, openwork pumice of U-4 tephra. **g** Accretionary lapilli-bearing tuff layers in the basal part of U-3 tephra. **h** Massive pumiceous lapilli tuff in the upper part of U-3 tephra, comprising subrounded to rounded pumice lapilli. **i** Accretionary lapilli-bearing tuff in the basal part of U-2 tephra. **j** Massive openwork pumice lapilli deposit in the upper part of U-2 tephra, comprising angular pumice lapilli

The U-Oki tephra occurs extensively with remarkable thickness (>5 cm) and shows densely populated openwork deposit texture of pumice lapilli identical to that of the stratigraphically equivalent terrestrial tephra. This feature suggests that the eruption was strong enough to sustain an extensive plinian eruption column, depositing a large volume of pumiceous tephra throughout the sea and over the Japanese Islands.

U-3 tephra (Unit N-3A and N-3C)

Description

U-3 tephra is a 1-m-thick tephra succession, comprising a lower accretionary lapilli-bearing tuff and an upper massive pumiceous lapilli tuff (Figs. 10 and 11). The lower part of the tephra is 0.3 m thick, showing parallel bedding defined by variations in the abundance and/or grain size of accretionary lapilli (Fig. 11g). The upper part of the tephra comprises subrounded to rounded, fine pumice lapilli and subordinate lithic lapilli, showing indistinctive grain size variation (Fig. 11h). The top of this tephra is locally scoured at low angle and overlain by matrix-supported lithic breccia containing rip-up clasts. Pumice clasts in this tephra are characterized by slightly stretched elliptical vesicles with thin vesicle walls (Fig. 5).

Interpretation

The accretionary lapilli-bearing tuff in the lower part, which shows very low lateral thickness variation, can be interpreted as a fallout deposit from a moist-rich ash cloud. The variation of grain size and/or abundance of the accretionary lapilli reflect pulsation of the eruption, accompanied by fluctuation of eruption intensity and water content in the ash cloud. The abrupt facies change up to the pumiceous lapilli tuff suggests a transition in eruption style from wet to dry. The high roundness of pumice clasts in the upper pumice-rich interval implies that the lapilli were significantly abraded during transport, which may indicate that the lapilli were initially transported within a PDC inside the caldera, and then deposited by fallout from a phoenix cloud that spilled out of the caldera rim (Branney and Kokelaar 1997; Branney and Kokelaar 2002).

The distinctive lithofacies such as the basal accretionary lapilli-bearing tuff and an overlying co-ignimbrite plume deposit, together with the existing radiocarbon ages (ranging from 8.3 to 9.0 ka B.P.; Okuno et al. 2010), suggest that U-3 tephra is equivalent to the intra-caldera Member N-3 (c. 8.3 ka B.P.; Im et al. 2012) (Table 3; Fig. 12). The basal accretionary lapilli-bearing tuff matches closely unit N-3A of the Nari Tephra Formation. It is inferred that the upper pumice-rich interval of U-3 is correlated with unit N-3C of the Nari Tephra

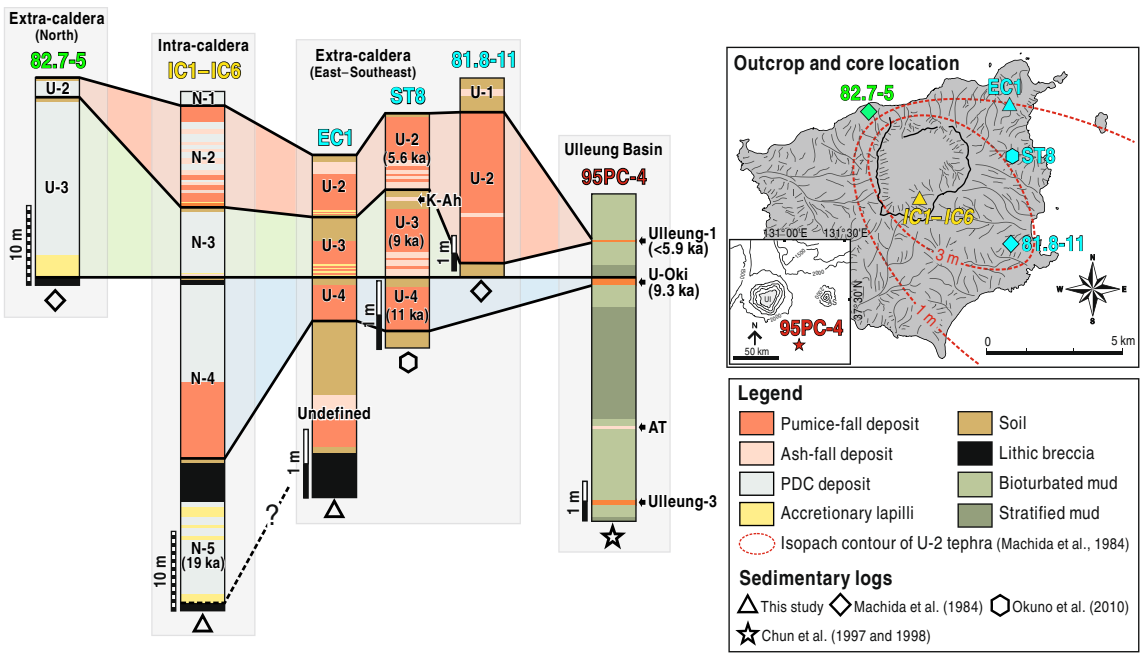

Fig. 12 Stratigraphic correlation of the Ulleung tephras between variable terrestrial and marine sequences in and around Ulleung Island. *Different colors* in simplified sedimentary logs represent different lithofacies. Map in the upper-right corner shows locations of each sedimentary logs and isopach contours of U-2 tephra (red dotted lines). Modified after Machida et al. (1984), Chun et al. (1997), Okuno et al. (2010), and Shiihara et al. (2011)

Formation, considering the fine grain size and rounded shapes of pumice lapilli.

U-2 tephra (Unit N-2A)

Description

U-2 tephra is a 1-m-thick tephra succession showing vertical facies change. The lower part is characterized by alternating, centimeter-thick accretionary lapilli-bearing tuff and pumiceous lapilli tuff layers showing mantling bed geometry (Fig. 11d, i). The upper part of the tephra consists of fine to coarse, angular pumice lapilli and subordinate lithic lapilli, showing openwork deposit texture (Fig. 11j). Pumice clasts in this tephra member show inflated bubble wall-type vesicle textures (Fig. 5).

Interpretation

Alternating accretionary lapilli-bearing tuff and openwork pumice lapilli layers in the lower part of U-2 tephra suggest fluctuations between phreatomagmatic and magmatic eruptions during the incipient eruption phase. The absence of accretionary lapilli tuff in the upper part of the unit shows that magma–water interaction was less important in the later phase of eruption. The angular clast shapes, openwork textures of pumice lapilli beds, and the mantling bed geometry of all units suggest deposition from a plinian eruption column. This facies association is identical to that of the lowermost unit of Member N-2 in the Nari Tephra Formation (unit N-2A), suggesting that Member N-2 and U-2 tephra are stratigraphically equivalent (Fig. 12).

Implication for transport/deposition processes of tephras beyond the Nari Caldera

Isopachs of the extra-caldera tephras equivalent to Member N-2 of the Nari Tephra Formation were mapped by Machida and Arai (1983) and suggest that the majority of the tephras from Ulleung Island were transported eastward or southeastward by the prevailing westerlies of this region (Fig. 12). However, the detailed field observation of the Nari Tephra Formation reveals that transport/deposition processes of the tephras were far more complicated than expected, suggesting roles of variable controlling factors besides the atmospheric winds.

Intra-caldera sites (IC1–IC6) preserve a more complete record of complex PDC and tephra-fall events associated with each eruptive phase, whereas extra-caldera sites preserve only a condensed record of either PDC or fall units depending on localities (Fig. 12). Most tephra deposits to the north of the caldera site (site 82.7-5) were deposited by PDCs, while the tephras to the eastern to southeastern parts (sites EC1, ST8, and 81.8-11) were deposited almost solely by fallout process (Fig. 12). This distribution suggests that both wind direction and also the morphology of the caldera were important controls of tephra dispersal beyond the caldera wall.

It is inferred that the eruption centers of individual tephra members as well as the sites of PDC generation due to eruption column collapse or fountaining eruption were confined inside the caldera. Thus, the PDCs could most readily flow out of the caldera only via its northern opening (Fig. 2a). On the other hand, the caldera rim is several hundred meters high in the eastern, western, and southern sectors, and was an effective topographic trap for the PDCs. The PDCs, upon climbing the lofty caldera walls, might have readily lost their inertia to escape the caldera, and also lost large portions of their particle load via deposition on the wall.

The double, overlapping semicircular rims in the south and the north of the Nari Caldera suggest successive formation of two collapsed depressions in different loci within the present extent of the caldera (Fig. 2). The restricted preservation of the Nari Tephra Formation in the southern embayment of the caldera suggests that the northern wall formed later, possibly in association with the latest set of eruptions. By repetitive caldera collapse in the north, the caldera as a whole gradually attained its present asymmetric geometry open to the north, which hindered tephra preservation in the northern depression.

Eruption history

The intra-caldera Nari Tephra Formation provides a new opportunity to reconstruct the eruptive history of Ulleung Island during the last 19,000 years, which has remained obscure in spite of a number of studies of marine and terrestrial tephras on the island, East Sea floor, and Japanese Islands. This study provides a detailed account of the eruptive processes and transport/deposition mechanisms of tephras, as well as of the geomorphic evolution of the caldera (Fig. 13).

Phreatomagmatic eruption associated with cryptodome disintegration (Member N-5)

The breccia succession beneath the Nari Tephra Formation suggests a long period of quiescence in the Nari Caldera, during which screes accumulated against the old caldera wall. After the quiescence, the volcano reawakened around 19 ka B.P. due to the interaction between ascending magma and ground or surface water to generate steam-rich eruption clouds in association with pulsating PDCs (N-5; Fig. 13a). The initial phreatomagmatic volcanism evolved into a magmatic explosive eruption (unit N-5B) that marks the climactic stage of the episode (Fig. 13b). Poor-vesicular and microlite-rich juvenile clasts in unit N-5B suggest that the climactic event was triggered by decompressional fragmentation of cryptodome

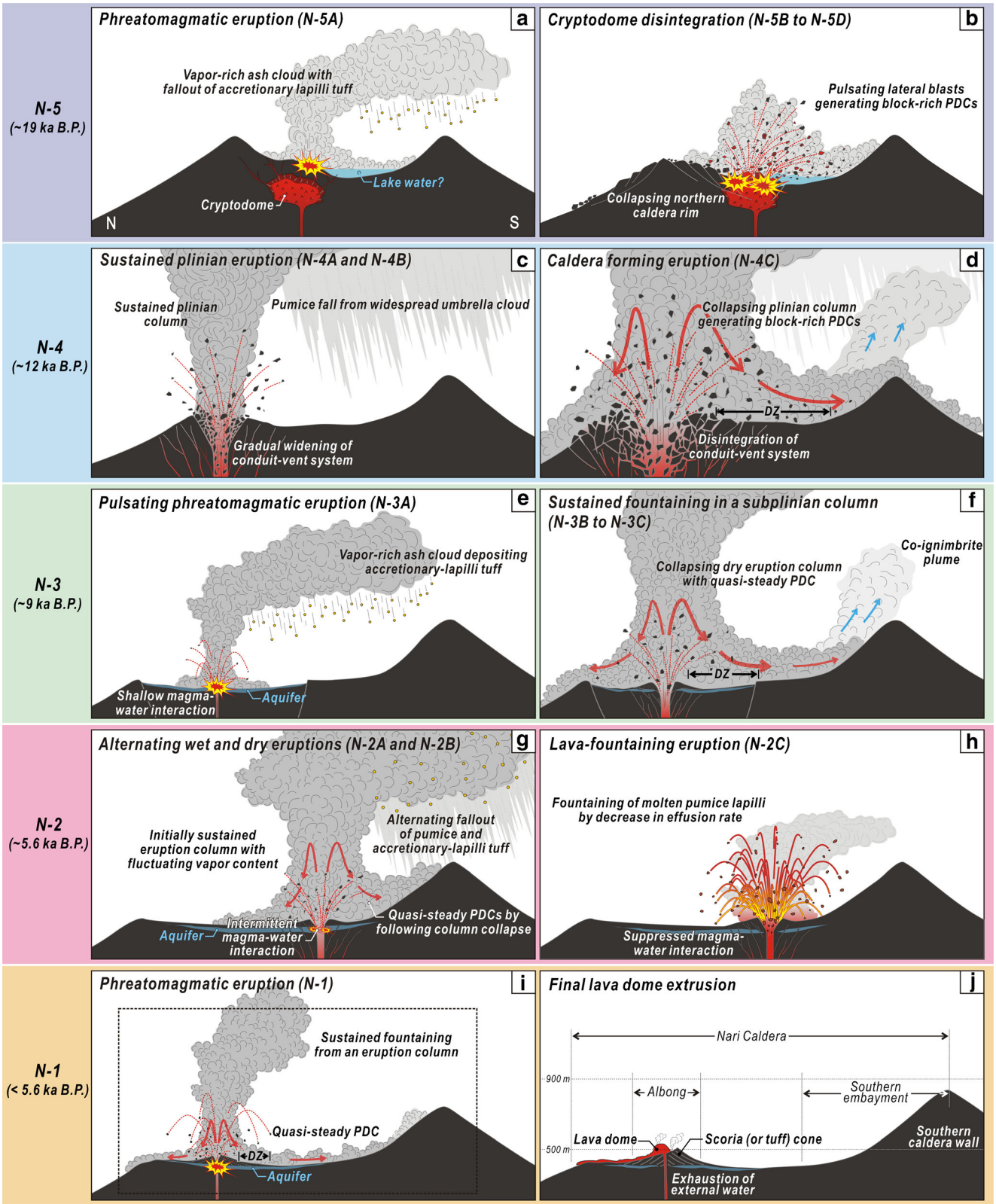

Fig. 13 Reconstruction of eruptive activities in Ulleung Island during the last 19,000 years. Each conceptual model illustrates eruption style, eruption intensity, and transport/deposition process of tephra. **a**, **b** The earliest eruption marked by initial phreatomagmatic eruptions followed by cryptodome disintegration at around 19 ka (Member N-5). **c**, **d** The strongest plinian eruption at around 11 ka followed by rapid vent widening and caldera collapse (Member N-4). **e**, **f** A sustained fountaining eruption in a subplinian column with precursory phreatomagmatic activities at around 9 ka (Member N-3). **g**, **h** A subplinian eruption gradually changing from wet to dry eruption at around 5.6 ka (Member N-2). **i**, **j** The final phreatomagmatic activity (Member N-1) followed by strombolian eruption and lava dome extrusion

or magma within the shallow conduit as the initial phreatomagmatic explosions. It is inferred that the partly degassed and crystal-rich viscous magma could not be subject to pure magmatic fragmentation, but was emplaced as an endogenous dome or a cryptodome infilling part of the caldera. We postulate that the initial phreatomagmatic eruption was caused by the interaction between cryptodome magma and external water infiltrating via surficial fractures, which subsequently triggered collapse and disintegration of the hot and gas-pressurized cryptodome (Heiken and Wohletz 1987; Hoblitt and Harmon 1993; Alidibirov 1995; Alidibirov et al. 1997; Alidibirov and Dingwell 2000).

The distinct phonolitic juvenile composition of the Member N-5 tephra suggests that it was erupted as a new phase distinguished from the earlier trachytic eruptions that formed the summit of Ulleung Island and stubby lava flows around the island (Brenna et al. 2014). The northern caldera wall probably began to collapse during this N-5 eruption, in part due to cryptodome emplacement near the northern margin of the pre-Nari Formation caldera (Figs. 13a, b). The disintegration of the cryptodome likely generated lateral blasts and block-rich PDCs southward, which piled up coarse lapilli tuff of unit N-5B on the southern inner walls of the caldera. Following the N-5B climactic stage, magma–water interaction resumed and resulted in repetitive deposition of tuff or lapilli tuff beds with variable ash-accretion textures through the upper part of Member N-5 (Fig. 13b). The repetitive phreatomagmatic eruptions in the later stage of the N-5 episode suggest the existence of a ready source of external water within the Nari Caldera, possibly a caldera lake, with similarities to the hydrovolcanic eruption at Taal caldera lake in 1991 (Delmelle and Bernard 2000), hydromagmatic eruption of Kilauea Volcano in 1970 (Mastin 1997), and Holocene explosive eruptions of Witori and Dakataua Caldera volcanoes (Machida et al. 1996), among others.

Plinian eruption followed by rejuvenated caldera collapse (Member N-4)

After the eruption of Member N-5, the volcano remained quiescent for almost 10,000 years. During this period, reworking of loosely consolidated pyroclastics and deposition of screes occurred on the caldera wall slopes. At around 8.3 ka B.P., the N-4 eruptive episode began, which was the largest and most explosive eruption recorded in the Nari Tephra Formation.

Initially, the eruption most likely involved short-lived phreatomagmatic activity, and deposited fine ash-rich lapilli tuff via PDCs that produced pinch-and-swell strata (unit N-4A). Afterward, the mass flux of the ascending magma increased dramatically, leading to a highly explosive magmatic eruption forming a plinian eruption column and widespread umbrella cloud (unit N-3B) (Fig. 13c). This produced rapid aggradation of coarse pumice lapilli, along with ballistic projectiles of vent- or conduit-derived lithic blocks. The commonly contorted tubular vesicle texture of the pumice clasts evidences strong applied shear during vesicle growth within the conduit due to rapid magma ascent rates along with still ductile melt (Cashman et al. 2000; Polacci et al. 2003).

In the studies of modern and ancient analogues of plinian or subplinian eruptions, it is broadly recognized that the initial sustained plinian columns begin to collapse in association with rapid widening of the conduit-vent system, development of pervasive permeable gas pathways in magma foams by stretching and coalescence of vesicles, or due to caldera or ring-fault collapse followed by depressurization of the magma chamber (e.g., Druitt and Sparks 1984; Heiken and McCoy 1984; Wilson and Walker 1985; Cioni et al. 2000; Polacci et al. 2003; Kawakami et al. 2007; Bear et al. 2009; Polacci et al. 2009). The sharp facies transition, identified in Member N-4 from a pumice lapilli fall unit (unit N-4B) to block-rich lapilli tuff and tuff breccia (unit N-4C), marks the change in eruption style from the column-sustaining eruptive phase to a column-collapsing phase (Fig. 13d) that presumably accompanied instability of the conduit-vent system. The high lithic content of the PDC deposits from this phase are consistent with caldera-forming eruptions although a sensu stricto ignimbrite lag deposit was not found. Considering that Member N-4 is the largest and most widespread unit found in marine (U-Oki tephra) and terrestrial tephra (U-4 tephra) records, it is likely that this episode was responsible for the further stepwise subsidence of the caldera in the north, overlapping the older caldera structure.

The block-rich PDC deposits on the inner caldera wall, deposited by upslope-moving currents, suggest a broad deflation zone of collapsing eruption column, generating proximal PDCs energetic enough to transport entrained large lithic blocks up and over the caldera wall. A wide range of sorting, pumice/lithic ratio, and grading pattern of unit N-4C is attributed to a highly fluctuating eruption that might have been sourced from several locations around a ring-fault structure, resulting in a range in PDC particle-concentration, steadiness, and intensity, as well as variations in the lithology and size of entrained country rock lithic blocks (Walker 1985; Branney and Kokelaar 2002).

Sustained low-column fountaining eruption following precursory phreatomagmatic activity (Member N-3)

After the cessation of the N-4 eruption, the volcano entered again a long period of quiescence (unit N-4R) at around 9 ka (Fig. 13e). The N-3 eruption episode started with a brief phreatomagmatic eruption. Pervasive erosion of the accretionary lapilli-bearing tuff (unit N-3A) suggests a significant eruption break of at least a few days to weeks, during which most of the friable ashfall deposits were reworked.

After the pause, a "dry" explosive eruption began with higher mass flux and a widening of the conduit-vent system. The member as a whole lacks the characteristics of tephra-fall deposition, which suggests a more or less sustained fountaining or "boiling over" type of eruption producing PDCs that fluctuated in steadiness and density (unit N-3B) (c.f., Taylor 1958) (Fig. 13f). The eruption gradually shifted to a phase of individual explosions, possibly along with lower magma mass ejection rates and possible return to magma–water interaction, generating dilute, turbulent-supported PDCs (unit N-3C).

PDCs traveling up the internal caldera wall during this stage produced a variety of upslope-oriented depositional/erosional structures (i.e., megaripples, dunes, flutes, and obstacle scours). However, the density-stratified PDCs probably also were accompanied by basal backflows separated from the upslope-directed currents during their passage (Piper and Normark 1983; Edwards et al. 1994; Jeon et al. 2011). Coarse-grained basal backflows were most likely deposited as fines-poor pumice lenses, whereas the fully dilute upper portion of the PDCs detached and could surmount caldera walls as a co-ignimbrite phoenix plume (Fig. 13f).

Transitional wet to dry eruption terminating with lava fountaining event (Member N-2)

Following approximately 3,000 years of quiescence, the volcano reawakened with explosive phreatomagmatic activity. During this stage, fluctuations between wet and dry eruptions deposited alternating pumice lapilli falls and accretionary lapilli-bearing tuff layers on intra-caldera and medial extra-caldera sites (Figs. 12 and 13g). The intermittent magma–water interaction was gradually suppressed, before a brief dry column-forming eruption that deposited coarse pumice fall units. This eruption column soon began to collapse, generating quasi-steady PDCs that deposited diffuse-bedded pumiceous lapilli tuff beds (unit N-2B). Deposition of brown and black pumice (the upper part of unit N-2B) was restricted to the intra-caldera sites only, implying that PDCs were not energetic enough to escape the caldera during the last phases.

At the final stage of the episode, eruption shifted to a fountaining phase, depositing agglutinated black pumice and obsidian clasts locally within the caldera. Considering the localized deposition range of such fountaining eruptions, the thick pile of agglutinated pumice on the southern slope of the caldera indicates that the source vent of the N-2 eruption was closer to the southern caldera than the vents of N-4 and N-3. (Fig. 13h).

The latest phreatomagmatic activity and lava dome extrusion (Member N-1 and Albong)

The last known eruptive episode of the Nari Tephra Formation commenced with explosive phreatomagmatic activity, generating dilute PDCs (Fig. 13i). The repetitive alternation of normal and inverse grading in Member N-1 suggests that the PDC fluctuated in current competence, causing stepwise aggradation of traction carpet strata (Sohn 1997; Branney and Kokelaar 2002). This tephra is not found outside the caldera, implying that the PDCs were primarily low-runout and confined by the caldera walls.

Younger pyroclastic deposits are not found above Member N-1 in the intra-caldera sites IC1 to IC6. However, a lava dome/tephra cone complex, Albong, located in the northern part of the present caldera, suggests multiple repeated effusive eruptions following the phreatomagmatic phase. Both the Albong lava/tephra and the juvenile components of Member N-1 have very similar plagioclase- and kaersutite-rich lithology, which are distinctive in this sequence. This indicates that their magma sources were highly likely to be similar. Thus, the final eruptive episode within the Nari Caldera had two eruptive phases, an earlier explosive phreatomagmatic eruption depositing Member N-1 (Fig. 13i) culminating in an effusive eruption, forming the tephra and lava dome complex (Fig. 13j).

Conclusion

The Nari Tephra Formation is an intra-caldera tephra sequence that records the most complete eruptive history during the last 19,000 years yet reported for the Ulleung Island volcano. Five eruptive episodes are recognized during this period, with a range of eruption styles and pyroclastic transport/deposition processes exhibited. The eruption history can be reconstructed as follows: (1) an eruption episode associated with cryptodome disintegration at around 19 ka B.P. (N-5); (2) the largest plinian eruption known from Ulleung at 11 ka B.P., followed by rapid vent widening and caldera collapse (N-4); (3) a sustained fountaining eruption with precursory hydrovolcanic activity at around 9 ka B.P. (N-3); (4) a subplinian eruption that gradually changed from wet to dry eruption at around 5.6 ka B.P. (N-2); and (5) the final hydrovolcanic activity (N-1) followed by strombolian-type eruption and lava dome extrusion. The logging and stratigraphic correlation of the Ulleung Island tephra reveal that the transport and deposition of tephra were controlled by the eruption style, locus of source vent, extent of deflation zone, caldera geometry, and dominant wind directions. In most column-collapsing and tephra-fountaining events, the deflation zone developed inside the caldera rim, which caused the majority of PDCs to be trapped within the caldera walls. Only the major sustained eruption columns and minor co-ignimbrite plume events deposited tephra beyond the caldera. In this study, sedimentological findings from intra-caldera tephra sequences complement the existing Ulleung tephrostratigraphy, as well as provide a deeper understanding

of eruption styles and controlling factors of tephra transport/deposition processes. Our reconstruction of the most recent eruptive history can aid evaluations of volcanic hazards at Ulleung Island.

Acknowledgments This work was supported by Basic Science Research Program to YKS (2009-0079427) through the National Research Foundation of Korea (NRF) funded by the Ministry of Education. We are grateful for the careful and constructive reviews and comments by Károly Németh and an anonymous reviewer and the editorial guidance by Clive Oppenheimer.

References

Alidibirov M, Dingwell DB (2000) Three fragmentation mechanisms for highly viscous magma under rapid decompression. J Volcanol Geotherm Res 100:413–421

Alidibirov M, Dingwell DB, Stevenson RJ, Hess K-U, Webb SL, Zinke J (1997) Physical properties of the 1980 Mount St. Helens cryptodome magma. Bull Volcanol 59:103–111

Alidibirov MA (1995) A model for the mechanism of the May 18, 1980 Mount St. Helens blast. J Volcanol Geotherm Res 66:217–225

Allen SR (2001) Reconstruction of a major caldera-forming eruption from pyroclastic deposit characteristics: Kos Plateau Tuff, eastern Aegean Sea. J Volcanol Geotherm Res 105:141–162

Arai F, Oba T, Kitazato H, Horibe Y, Machida H (1981) Late Quaternary tephrochronology and paleo-oceanography of the sediments of the Japan Sea. Quat Res 20(3):209–230

Basu AR, Huang WK, Zie GH, Tatsumoto M (1991) Major element, REE, and Pb, Nd, and Sr isotopic geochemistry of Cenozoic volcanic rocks of Eastern China: implications for origin from suboceanic-type mantle reservoirs. Earth Planet Sci Lett 105:149–169

Bear AN, Cas RAF, Giordano G (2009) The implications of spatter, pumice and lithic clast rich proximal co-ignimbrite lag breccias on the dynamics of caldera forming eruptions: the 151 ka Sutri eruption, Vico Volcano, Central Italy. Journal of Volcanology and Geothermal Researc 181(24):1–24

Branney MJ, Kokelaar P (1997) Giant bed from a sustained catastrophic density current flowing over topography: Acatlán ignimbrite, Mexico. Geology 25:115–118

Branney MJ, Kokelaar P (2002) Pyroclastic density currents and the sedimentation of ignimbrites. Geological Society Meoirs No. 27. Geological Society, London, p 143

Brenna M, Price R, Cronin SJ, Smith IEM, Sohn YK, Kim GB, Maas R (2014) Final magma storage depth modulation of explosivity and trachyte/phonolite genesis at an intraplate volcano: a case study from Ulleung Island, Republic of Korea. J Petrol. doi:10.1093/petrology/egu004

Cashman KV, Sturtenvant B, Papale P, Navon O (2000) Magmatic fragmentation. In: Sigurdsson H (ed) Encyclopedia of volcanoes. Academic, San Diego, pp 421–430

Chun JH, Han SJ, Cheong DK (1997) Tephrostratigraphy in the Ulleung Basin. East Sea: Late Pleistocene to Holocene. Geosci J 1(3):154–166

Chun JH, Han SJ, Cheong DK, Huh S, Bahk JJ, Choi DL (1998) Tephrostratigraphy of deep-sea sediments around submarine channels, northeastern Ulleung Basin. J Geol Soc Korea 34:192–210

Cioni R, Marianelli P, Santacroce R, Sbrana A (2000) Plinian and subplinian eruptions. In: Sigurdsson H (ed) Encyclopedia of volcanoes. Academic, San Diego, pp 477–511

Delmelle P, Bernard A (2000) Volcanic lakes. In: Sigurdsson H (ed) Encyclopedia of volcanoes. Academic, San Diego

Domitsu H, Shiihara M, Torii M, Tsukawaki S, Oda M (2002) Tephrostratigraphy of the piston cored sediment KT96-17 P-2 in the southern Japan Sea: the eruption age of Daisen-Kusadanihara Pumice (KsP). J Geol Soc Jpn 108(9):545–556

Druitt TH, Sparks RSJ (1984) On the formation of calderas during ignimbrite eruptions. Nature 310:679–681

Edwards DA, Leeder MR, Best JL, Pantin HM (1994) On experimental reflected density currents and the interpretation of certain turbidites. Sedimentology 41:437–461

Hammer JE, Cashman KV, Hoblitt RP, Newman S (1999) Degassing and microlite crystallization during pre-climactic events of the 1991 eruption of Mt. Pinatubo, Philippines. Bull Volcanol 60:355–380

Heiken G, McCoy F (1984) Caldera development during the Minoan eruption, Thira, Cyclades, Greece. J Geophys Res 89:8441–8462

Heiken G, Wohletz K (1987) Tephra deposits associated with silicic domes and lava flows. Geol Soc Am Bull 212:55–76

Higashino T, Tsujimori T, Itaya T (2005) An alkaline tephra found at Midagahara, Mt. Hakusan. 32. Ann Report Hakusan Nat Conserv Center 32:1–7

Hoblitt RP, Harmon RS (1993) Bimodal density distribution of cryptodome dacite from the 1980 eruption of Mount St. Helens, Washington. Bull Volcanol 55:421–437

Houghton BF, Wilson CJN, Smith RT, Gilbert JS (2000) Phreatoplinian eruptions. In: Sigurdsson H (ed) Encyclopedia of volcanoes. Academic, San Diego, pp 513–525

Im JH, Choo CO, Jang YD (2011) Petrological and mineralogical characteristics of matrix of pumice in Ulleung Island. J Mineral Soc Korea 24(3):151–164

Im JH, Shim SH, Choo CO, Jang YD, Lee JS (2012) Volcanological and paleoenvironmental implications of charcoals of the Nari Formation in Nari Caldera, Ulleung Island, Korea. Geosci J 16(2):105–114

Jeon YM, Kwon CW, Sohn YK (2011) Deposition from pyroclastic surges partially blocked by a topographic obstacle: an example from the Ilchulbong tuff cone, Jeju Island, Korea. Geosci J 15(2):121–130

Jolivet L (1986) American–Eurasia plate boundary in eastern Asia and the opening of marginal basins. Earth Planet Sci Lett 81:282–288

Kawakami Y, Hoshi H, Yamaguchi Y (2007) Mechanism of caldera collapse and resurgence: observations from the northern part of the Kumano Acidic Rocks, Kii peninsula, southwest Japan. J Volcanol Geotherm Res 167:263–281

Kim GB, Yoon SH, Chough SK, Kwon YK, Ryu BJ (2011) Seismic reflection study of acoustic basement in the South Korea Plateau, the Ulleung Interplain Gap, and the northern Ulleung Basin: volcano-tectonic implications for Tertiary back-arc evolution in the southern East Sea. Tectonophysics 504:43–56

Kim GB, Yoon SH, Sohn YK, Kwon YK (2013) Wave-planation surfaces in the mid-western East Sea (Sea of Japan): indicators of subsidence history and paleogeographic evolution of back-arc basin. Mar Geol 344:65–81

Kim KH, Tanaka T, Nagao K, Jang SK (1999) Nd and Sr isotopes and K-Ar ages of the Ulreungdo alkali volcanic rocks in the East Sea, South Korea. Geochem J 33:317–341

Kim YK (1985) Petrology of Ulreung volcanic island, Korea—part 1 Geology. J Mineral Petrol Econ Geol 80:128–135

Kim YK, Lee DS (1983) Petrology of alkali volcanic rocks in northern part of Ulleung Island. Min Geol 1:19–36

Kimura G, Tamaki K (1986) Collision, rotation, and back-arc spreading in the region of the Okhotsk and Japan Seas. Tectonics 5:389–401

Kitagawa H, Fukusawa H, Nakamura T, Okamura M, Takemura K, Hayashida A, Yasuda Y (1995) AMS 14C dating of varved sediments from Lake Suigetsu, central Japan and atmospheric 14C change during the late Pleistocene. Radiocarbon 37:371–378

Lallemand S, Jolivet L (1985) Japan sea: a pull-apart basin. Earth Planet Sci Lett 76:375–389

Machida H, Arai F (1983) Extensive ash falls in and around the Sea of Japan from large late Quaternary eruptions. J Volcanol Geotherm Res 18:151–164

Machida H, Arai F, Lee BS, Moriwaki H, Furuta T (1984) Late Quaternary tephras in Ulreung-do Island, Korea. J Geog 93(1):1–14

Machida H, Blong RJ, Specht J, Moriwaki H, Torrence R, Hayakawa Y, Talai B, Lolok D, Pain CF (1996) Holocene explosive eruptions of Witori and Dakataua Cladera volcanoes in west New Britain, Papua New Guinea. Quat Int 34–36:65–78

Mastin LG (1997) Evidence for water influx from a caldera lake during the explosive hydromagmatic eruption of 1790, Kilauea volcano, Hawaii. J Geophys Res 102:20093–20109

Min KD, Kim OJ, Yoon S, Lee DS, Kim KH (1988) Applicability of plate tectonics to the post-Late Cretaceous Igneous activity and mineralization in the southern part of South Korea (II). J Geol Soc Korea 24: 11–40

Miura K, Ikehara K, Kikkawa K (1991) Volcanic ashes derived from Daisen volcano in the subsurface deposits of Japan Sea, off the coast of Hokuriku region Studies of the San'in Region, vol. 7. Center for studies of the San'in region, Shimane University, pp. 7–22.

Nagahashi Y, Yoshikawa S, Miyakawa C, Uchiyama T, Inouchi Y (2004) Stratigraphy and chronology of widespread tephra layers during the past 430 ky in the Kinki District and the Yatsugatake Mountains: major element composition of the glass shards using EDS analysis. The Quaternary Research (Daiyonki-Kenkyu) 43: 15–35

Okuno M, Shiihara M, Torii M, Nakamura T, Kim KH, Domitsu H, Moriwaki H, Oda M (2010) AMS radiocarbon dating of Holocene tephra layers on Ulleung Island, South Korea. Radiocarbon 52(6): 1465–1470

Park MH, Kim JH, Kil YW (2007) Identification of the late Quaternary tephra layers in the Ulleung Basin of the East Sea using geochemical and statistical methods. Mar Geol 244:196–208

Paulick H, Franz G (1997) The color of pumice: case study on a trachytic fall deposit, Meidob volcanic field, Sudan. Bull Volcanol 59:171–185

Peng ZC, Zartman RE, Futa K, Chen DG (1986) Pb-, Sr-, and Nd-isotopic systematics and chemical characteristics of Cenozoic basalts, eastern China. Chem Geol 59:3–33

Piper DJ, Normark WR (1983) Turbidite depositional patterns and flow characteristics, Navy Submarine Fan, California Borderland. Sedimentology 30:681–694

Polacci M, Baker DR, Mancini L, Favretto S, Hill RJ (2009) Vesiculation in magmas from Stromboli and implications for normal Strombolian activity and paroxysmal explosions in basaltic system. J Geophys Res 114:B01206

Polacci M, Pioli L, Rosi M (2003) The Plinian phase of the Campanian Ignimbrite eruption (Phlegrean Fields, Italy): evidence from density measurements and textural characterization of pumice. Bull Volcanol 65:418–432

Rosi M (1992) A model for the formation of vesiculated tuff by the coalescence of accretionary lapilli. Bull Volcanol 54:429–434

Schumacher R, Schmincke H-U (1991) Internal structure and occurrence of accretionary lapilli—a case study at Laacher See Volcano. Bull Volcanol 53:612–634

Shiihara M, Torii M, Okuno M, Domitsu H, Nakamura T, Kim KH, Moriwaki H, Oda M (2011) Revised stratigraphy of Holocene tephras on Ulleung Island, South Korea, and possible correlatives for the U-Oki tephra. Quat Int 246:222–232

Sohn YK (1997) On traction-carpet sedimentation. J Sediment Res 67(3): 502–509

Sohn YK, Park KH (1994) Geology and evolution of Tok Island. J Geol Soc Korea 30:242–261

Song YS, Park KH, Park ME (1999) Major, rare-earth and trace geochemistry of Ulleungdo volcanic rocks. J Petrol Soc Korea 8(2):57–70

Song YS, Park ME, Park KH (2006) Ages and evolution of the volcanic rocks from Ulleung-do and Dok-do. J Petrol Soc Korea 15:72–80

Sparks RSJ (1997) Causes and consequences of pressurisation in lava dome eruptions. Earth Planet Sci Lett 150:177–189

Tamaki K, Honza E (1991) Global tectonics and formation of marginal basins: role of the western Pacific. Episodes 14:224–230

Tamaki K, Suyehiro K, Allan J, Ingle JC, Pisciotto KA (1992) Tectonic synthesis and implications of Japan Sea ODP Drilling Program, 127/128, Part 2, Scientific Results. pp 1333-1348

Tatsumoto M, Nakamura Y (1991) DUPAL anomaly in the Sea of Japan: Pb, Nd, and Sr isotopic variations at the eastern Eurasian continental margin. Geochim Cosmochim Acta 55:3697–3708

Taylor GAM (1958) The 1951 eruption of Mount Lamington, Papua. Goelogy and Geophysics, 38. Department of Resources and Energy, Bureau of Mineral Resources, p 129

Walker GPL (1985) Origin of coarse lithic breccias near ignimbrite source vents. J Volcanol Geotherm Res 25:157–171

White JDL, Houghton BF (2000) Surtseyan and related phreatomagmatic eruptions. In: Sigurdsson H (ed) Encyclopedia of volcanoes. Academic, San Diego, pp 477–494

Wilson CJN, Houghton BF (2000) Pyroclast transport and deposition. In: Sigurdsson H (ed) Encyclopedia of volcanoes. Academic, San Diego

Wilson CJN, Walker GPL (1985) The Taupo eruption, New Zealand. Philos Trans R Soc London, Ser A 314:199–228

Won JK, Lee MW (1984) The volcanism and petrology of alkali volcanic rocks, Ulrung Island. J Geol Soc Korea 20(4):296–305

Xu S, Uto K, Kim K (1998) K-Ar dating of volcanic rocks from Ulreung Island, Korea. Geochem J 32:117–123

Yoon S (1984) Volcanism and tectonics of Ulleung Island, Korea, with a note on the formation of the Japan sea. In: Tsuchi R (ed) Pacific Neogene events in time and space. IGCP-246, pp 1-9

Yun HD (1986) The geochemical characteristics and origin of alkaline magmas in the Ulleung Island, Korea, Ph.D. dissertation. In: Seoul National University, Seoul, p 172, http://s-space.snu.ac.kr/handle/10371/58507